DR MANSOUR M. ABDELMALAK (Orcid ID : 0000-0003-2200-1074)

Article type : Original Article

The thermal maturity of sedimentary basins as revealed by magnetic mineralogy

M.M. Abdelmalak[1,2*], S. Polteau[3,4]

[1]Centre for Earth Evolution and Dynamics (CEED), University of Oslo, Norway

[2] Research Centre for Arctic Petroleum Exploration (ARCEx) University of Tromsø, Norway

[3] Institute for Energy Technology (IFE), Kjeller, Norway

[4] SurfExGeo, 0776 Oslo, Norway

*corresponding author: m.m.abdelmalak@geo.uio.no / abdelmalak_mansour@yahoo.fr

Abstract

The thermal evolution of sedimentary basins is usually constrained by maturity data, which is interpreted from Rock-Eval pyrolysis and vitrinite reflectance analytical results on field or boreholes samples. However, some thermal evolution models may be inaccurate due to the use of elevated maturities measured in samples collected within an undetected metamorphic contact aureole surrounding a magmatic intrusion. In this context, we investigate the maturity and magnetic mineralogy of 16 claystone samples from Disko-Svartenhuk Basin, part of the SE Baffin Bay volcanic margin. Samples were collected within thermal contact metamorphic aureoles near magma intrusions, as well as equivalent reference samples not affected by intrusions. Rock-Eval pyrolysis (Tmax), and vitrinite reflectance (Ro) analysis were performed to assess the thermal maturity, which lies in the oil window when 435°C≤Tmax≤470°C and 0.6-0.7%≤Ro≤1.3%. In addition, we performed low (<300K) and high temperature (>300K) investigations of isothermal remanent magnetization to assess the magnetic mineralogy of the selected samples. The maturity results (0.37%≤Ro≤2%, 22°C≤T_{max}≤604°C) show a predominance of immature to early mature Type III organic matter, but do not reliably identify the contact aureole when compared to the reference samples. The magnetic assemblage of the immature samples consists of iron sulfide (greigite), goethite, and oxidized or non-stoichiometric magnetite. The magnetic assemblage of the early mature to mature samples consists of stoichiometric magnetite and fine-grained pyrrhotite (<1 μm). These results document the disappearance of the iron sulfide (greigite) and increase in content of magnetite during normal burial. On the other hand, magnetite is interpreted to be the dominant magnetic mineral inside the contact aureole surrounding dyke/sill intrusions where paleotemperatures indicate mature to over-mature state. Interestingly, the iron sulfide (greigite) is still detected in the contact aureole where paleotemperatures exceeded 130°C. Therefore, the magnetic mineralogy is a sensitive method that can characterize normal burial history, as well as identify hidden metamorphic contact aureoles where the iron sulfide greigite is present at temperatures beyond its stability field.

Keywords: thermal maturity, magnetic mineralogy, claystones, burial depth, magma intrusion.

1. Introduction

The thermal evolution of sedimentary basins is often modelled based on maturity parameters extracted from field or well data (e.g., Haxby et al., 1976; Welte and Yukler, 1981; Palumbo et al., 1999). When considering organic-rich rocks, Rock-Eval pyrolysis (Tmax) and the vitrinite reflectance (Ro) are standard geothermometers that provide parameters to infer the maturity of organic matter (e.g., Espitalié et al., 1986; Burnham and Sweeney, 1989; Bordenave, 1993; Suggate, 1998). However, both methods have significant

uncertainties in terms of estimated temperatures; which are often the results of different maturities that are measured on both re-worked and in situ organic matter in the same sample (Sweeney and Burnham, 1990). In addition, both methods are also lithology-specific and are mostly restricted to organic-rich sediments such as claystones, siltstones, and marls. Furthermore, thermal modelling is more complex in volcanic basins, which are sedimentary basins intruded by large volumes of magma. Indeed, the maturation levels of volcanic basins can vary locally or on a basin-scale depending on the duration, number, and timing of successive emplacement events, fluid and organic type and content in the country rocks, as well as structuring and lithological properties influencing hydrothermal circulations patterns (Aarnes et al., 2010). In addition to contact metamorphism, the thermal maturation of strata in volcanic basins is also a product of burial. Therefore, using thermal indicators that are independent to the type and composition of organic matter would provide better maturity constrains where the standard geothermometers fail.

The aim of this study is to constrain the maturity history of sedimentary sequences based on their magnetic mineralogy to distinguish if maturity is due to normal burial or is a combination of burial and contact metamorphism around magmatic intrusions. The magnetic mineralogy approach must be sensitive enough to identify rocks within a contact aureole, even if no intrusive has been intersected by drilling. Our rationale is based on the principle that the formation of new minerals carrying a remanent chemical magnetisation reflects the thermal history of a rock (e.g., Kars et al., 2012; Aubourg et al., 2014). In particular, changes in magnetic assemblages are often the result of precipitation of iron that is released during the alteration of pyrite (Brothers et al., 1996) or clays (Katz et al., 1998) during early diagenesis (Roberts and Weaver, 2005; Rowan and Roberts, 2006; Rowan et al., 2009; Roberts, 2015), thermal maturation of sedimentary rocks (Banerjee et al., 1997) and increasing burial (Aubourg et al., 2012). Laboratory experiments have demonstrated that heating claystones from 50° C to 250 °C leads to the formation of new magnetic minerals (Cairanne et al., 2004; Moreau et al., 2005; Aubourg et al., 2008; Aubourg and Pozzi, 2010; Kars et al., 2012), with greigite, goethite, magnetite and pyrrhotite defining the contours of the magnetic diagenesis (Aubourg et al., 2012). In natural conditions, greigite is derived from the microbial alteration of detrital iron oxides in the anoxic environment that is located up to several tens of meters below the surface (Roberts et al., 2011). Goethite is also present in immature claystones in which burial temperatures did not exceed 90°C (e.g., Abdelmalak et al., 2012a). Burial re-magnetization is interpreted to be controlled by the crystallization of ultra-fine-grained stable single domain (SD) superparamagnetic (SP) magnetite between 50 °C to 250 °C (Aubourg and Pozzi, 2010; Kars et al., 2012). Coincidentally, the formation of magnetite falls within the temperature range of the oil generation window, which is between 60-90°C to 120–150°C (e.g., Elmore et al., 1987; Jackson et al., 1988; McCabe et al., 1989; Katz et al., 2000; Elmore et al., 2006). Fine-grained monoclinic pyrrhotite forms from 150 °C to ~ 350 °C (e.g., Aubourg and Pozzi, 2010; Roberts, 2015). All of these neoformed minerals coexist in

ranges of depths that are still not resolved. For example, greigite becomes unstable at temperatures above 200 °C, which corresponds to a burial depth >8 km for a geothermal gradient of 25°C/km (Roberts et al., 2011). In addition, magnetite is consumed during the formation of micron-sized pyrrhotite, and may totally be absent at depths >12 km. Consequently, these newly formed magnetic minerals have been used as proxies for interpreting the burial history of sedimentary formations (Bishop and Abbott, 1995).

In the case of sedimentary basins affected by volcanism, several studies have connected the occurrences of magnetite, hematite, and pyrrhotite with specific degrees of thermal and hydrothermal alteration in the contact metamorphic aureoles surrounding individual sill and dyke intrusions (e.g., Katz et al., 1998; Gillett, 2003; Aubourg et al., 2014) or around larger intrusions (Just et al., 2004; Petronis et al., 2011). Indeed, the formation of these magnetic minerals is controlled by the fugacity of oxygen and sulfur that are specific to thermal aureoles (Gillett, 2003). Alternatively, recognizing these diagnostic minerals can help to identify hidden thermal aureoles developed in clay-dominated sedimentary sequences (mud-stones, claystones and siltstones).

In this contribution we present a detailed rock magnetic study on reference Cretaceous/Palaeocene claystones from the SE-Baffin Bay not affected by volcanism, as well as on equivalent sedimentary sequences intruded by magmatic dykes and sills. For comparison, we further used the standard Rock-Eval pyrolysis and vitrinite reflectance analyses to evaluate the thermal evolution of the sedimentary basin. Our results are relevant for hydrocarbon exploration since potential source rock intervals may be over-mature in the aureole, and in the oil window few tens of meter away. Therefore, the magnetic mineralogy approach should help to avoid misinterpreting the anomalous contact metamorphic maturities as representing the burial history of a basin.

2. Geological setting and burial history

The Disko-Svartenhuk Basin is located in Central West Greenland at the termination of the SE Baffin Bay volcanic margin, (Geoffroy, 2001; Abdelmalak, 2010; Abdelmalak et al., 2012b). The geological record and apatite fission track data indicate that the Disko-Svartenhuk Basin was uplifted and eroded during several episodes in the Cenozoic (Japsen et al., 2005; Bonow et al., 2006; Japsen et al., 2006; Japsen et al., 2009; Japsen et al., 2010). Consequently, the border faults along the basement, the Cretaceous-early Paleocene sedimentary strata, and the overlapping and sealing of the sedimentary basin by Paleogene volcanism are exposed on land in an area of about 200 by 300 km (e.g., Abdelmalak et al., 2019). The Central West Greenland is a unique area with excellent exposures that documents in outcrop the transition between a sedimentary basin to a volcanic-type passive margin.

The Cretaceous sedimentary sequences form a delta system that fanned out from Disko (in the south) to the West and the North-West of Nuussuaq (e.g., Chalmers and Pulvertaft, 2001; Dam et al., 2009) (Fig. 1). The Albian proximal fluvial Kome Formation (sample G46) and the lacustrine Slibestensfjeldet Formation (sample G14, Fig. 1a) are the oldest exposed sediments. The Albian to early Campanian period is characterized by the deposition of the fluvio-deltaic Atane Formation in Disko and Nuussuaq (sample G19 in the north and samples G49, G50 and G51, Fig. 1b) to the south, and the Upernivik Næs Formation to the north (e.g., Dam et al., 2009). The proximal near coastal areas of Upernivik Næs Formation claystones were sampled in Upernivik Ø (samples G20 and G44), in Qeqertarsuaq Island (sample G33) and at Itsaku (sample G31). Northward, the fluvio-deltaic facies of the Atane Formation becomes the time equivalent of the distal deep marine claystones of the Itilli Formation, which is exposed in the north of Nuussuaq (samples G15 and G48) and in Svartenhuk Halvø (samples G29 and G38).

The Maastrichtian to Lower Paleocene was a tectonically active period witnessing the uplift and erosion of the underlying sediments (Dam et al., 2000). An uplift over than 1.3 km is interpreted to reflect the impact of the Iceland plume in the early Paleocene (Dam et al., 1998a). This uplift was responsible for the formation of subaerial incised valleys that are connected to a submarine canyon system to the west (Dam et al., 2000; Dam, 2002). Sediments filling the valleys correspond to the proximal Quikavsak Formation, while the distal and marine sediments are referred to the Agatdalen and Kangilia formations in Itsaku (sample G25). This early Paleocene uplift event was followed by rapid subsidence of at least 1 km (Japsen et al., 2005) just before the extrusion at ~ 62 Ma of the Paleocene hyaloclastites into a residual lacustrine basin, and the subaerial lava sequences of Vaigat and Maligât Formations (Fig. 11) (e.g., Abdelmalak et al., 2019). The volcanic front moved eastward giving rise to the syn-volcanic lacustrine deposits of the Atanikerluk Formation (sample G52). The presence of the marine sediments within the Palaeogene sequence on Disko and Nuussuaq, exposed today at 1 km above sea level, demonstrates that the Palaeocene subsidence was followed by a major post-Palaeocene uplift (Piasecki et al., 1992; Green et al., 2011).

The apatite fission track data from Nuussuaq and Disko indicate a minimum of three cooling episodes during Cenozoic times (e.g., Japsen et al., 2005). The first episode occurred during the Eocene-Oligocene transition (36-30 Ma) after the Paleocene–Eocene post-rift subsidence episodes. The paleogeothermal gradient for this first episode was estimated to be between 40 and 50°C/km (Japsen et al., 2005). The other two cooling episodes occurred at 11-10 and 7-2 Ma in the late Neogene (Green, 2003; Japsen et al., 2005; Bonow et al., 2006; Japsen et al., 2009). The paleogeothermal gradient during these two periods of exhumation decreased to a value close to the present 30°C/km (Japsen et al., 2006). The 1.5 to 2 km of eroded section was estimated based on fission track data, which agrees well with the ca. 1.9 km thickness based on vitrinite reflectance data of Bojesen-Koefoed et al. (1997) from the Gro-3 well (see location in Fig. 1a).

3. Methods

3.1. Sampling strategy

The sampling strategy was designed to characterize the magnetic mineralogy of claystones affected by contact metamorphism around sill and dyke intrusions; hence we also collected reference samples that recorded the background thermal history of the Disko-Svartenhuk Basin before and during magmatism. Furthermore, we sampled the sedimentary basin from the proximal continental and shallow marine formations to the distal and deeper marine settings in the different parts of the basin to characterize the magnetic mineralogy with increasing burial depth (Table 1). The quality of the outcrops in Greenland is excellent, which allowed us to collect fresh claystone samples away from weathering effect of running water from rivers and streams, or any fluid contamination from fracture zones.

For samples collected within the metamorphic contact aureoles of magmatic intrusions, we chose proximal continental claystones from Qeqertuarssuq (G33) and Upernavik Ø (G44), and distal marine samples from Itsaku (in Svatenhuk Halvø peninsula) (G25 and G29) (Fig. 2). Samples G20 and G44 belong to the same sedimentary formation and were sampled at the same stratigraphic level (Table 1). However sample G44 is located between two dykes with a thickness of 3 m and 3.5 m respectively. The distance between these two dykes is about 5 m. Sample G25 was located at ~15 to 20 m above a sill thicker than 20 m. Sample G29 was collected 5 m above a ~10 m thick sill. Sample G33 was sampled in Qeqertarsuaq island, few hundred meters away from a kilometer scale dolerite intrusion or laccolith (Fig. 2). We assumed that all of these samples collected within two thickness of an intrusion are within the contact aureole, which can vary between 30% and 250% of the intrusion thickness (e.g., Aarnes et al., 2010). Based on visual inspections, we avoided sampling too close to the intrusion in order to prevent any hydrothermal alteration that could complicate the magnetic records (e.g., Katz et al., 1998). Here, all the distances separating a sample from the closest intrusion are maximum estimates, and hence include the possibility of a closer hidden intrusion that could be buried behind the outcrop surface. From the collected material, we selected 16 claystone samples for thermal maturity assessment by Rock-Eval pyrolysis (Tmax), vitrinite reflectance (Ro) and magnetic mineralogy (Fig. 1).

3.2. Rock-Eval and vitrinite reflectance

Total Organic Carbon (TOC in wt%), Hydrogen Index (HI in mg of HC/g TOC where HC stands for hydrocarbons), Oxygen Index (OI in mg of CO_2/g TOC) and Tmax (expressed in °C) were determined by Rock-Eval pyrolysis with a model 6 device from the Vinci Technologies (Lafargue et al., 1998) (Table 1) at ISTO (Institut des Sciences de la Terre d'Orléans, University of Orleans, France). The analyses were carried out on 100 mg of crushed samples under standard conditions. Tmax is the temperature at maximum

pyrolytic hydrocarbon generation and varies as a function of the natural thermal maturity of the organic matter (e.g., Espitalié et al., 1986). A petrographic study of the organic matter was performed using a Leica DMR XP microscope under reflected light using an oil immersion objective (x50), following the International Committee for Coal Petrology procedure (ICCP, 1971). This study determines the type and shape of organic matter, and measure reflectance of vitrinite particles in each sample. The vitrinite reflectance measurement is one of the most widely used parameters for thermal reconstruction of sedimentary basins maturation, where temperature and time are considered as the main factors influencing vitrinite reflectance values (Burnham and Sweeney, 1989). One of the main uncertainties related to vitrinite reflectance measurements is if the vitrinite is in situ or reworked (Lo, 1992) (Fig. 3). Autochthonous vitrinite particles are mainly characterized by angular fragments generally larger than 50 µm (Lo, 1992) (Fig. 3), and often contain framboid pyrite inclusions. Reworked vitrinites particles are smaller than 50 µm, display a rounded shape attributed to extensive transport, and never contain framboid pyrite inclusions. Particles smaller than 15 µm² are not taken into account in the measurements. The vitrinite reflectance values are reported in Table 1 with a fair to good confidence, and are based on a total of 100 random measurements on in situ vitrinite per sample.

3.3. Magnetic mineralogy measurements

In this section, we present the methods from a series of different magnetic measurements performed at room temperature, high-temperature above 300 Kelvins (K) (performed at the University of Cergy Pontoise, France) and low-temperature below 300 Kelvins (K) (performed at the Institute of Néel, Paris, France) for the selected 16 claystones. The magnetic mineralogy is characterized without ambiguity based on prominent magnetic transitions at specific temperatures in the demagnetization curves at high temperature (HT, >300K) and low-temperature (LT, <300K), while room temperature experiments provide variations in magnetic contents and mineralogy.

3.3.1 Room temperature (RT) experiments

The natural remanent magnetization (NRM), the magnetic susceptibility (χ), and the isothermal remanent magnetization (IRM) were measured at room temperature (Table 2). The NRM and IRM are measured using a JR6 spinner magnetometer (Agico-Ltd). The susceptibility (χ) was measured on bulk samples with KLY3-CS3 Kappabridge apparatus operating in a weak magnetic field of 4.10^{-4} T at the basic frequency of 920 Hz with a sensibility of 5.10^{-8} SI. The susceptibility (χ) is used to determine variations in magnetic content. The IRM was imparted by an impulse magnetizer ASC SCIENTIFIC model IM0 following Lowrie's protocol (1990) along x, y, z axes of a standard 10.8 cc core at 0.1 Tesla (low), 0.5 Tesla (medium), and 1.2 Tesla (strong) magnetic fields respectively to obtain information about the magnetic mineralogy. This device allows to define saturation curves up to 1.7 T.

3.3. 2. High-temperature (HT) experiments

The temperature dependency of remanence is probably the best method to identify trace amounts of magnetic minerals, in particular monoclinic pyrrhotite and magnetite at ~320°C and ~580°C (the Curie temperature), respectively (e.g., Dunlop, 1995; Dunlop and Özdemir, 1997). The IRM acquired at room temperature is thermally demagnetized at HT using a magnetically shielded in-house built furnace. Temperatures were increased at 25°C or 50°C steps from room temperature to 600°C. Thermal demagnetization reveals the spectrum of unblocking temperature and coercivity, which are diagnostic of magnetic minerals.

3.3. 3. Low-temperature (LT) experiments

Low-temperature experiments prevent the chemical transformations from heating above room temperature (e.g., van Velzen and Zijderveld, 1992), and hence are well-adapted for identifying the magnetic assemblage in rocks where organic matter coexists with iron sulfides. At low temperature, stoichiometric magnetite is firmly identified by the Verwey transition at ~ 120 K (e.g., Özdemir et al., 2002). This transition is the expression of a solid-state phase change from cubic above 120 K to monoclinic below 120 K (e.g., Muxworthy and McClelland, 2000; Walz, 2002). Pyrrhotite is characterized by a magnetic Besnus transition at ~35 K (Dekkers, 1989; Rochette et al., 1990). Aubourg and Pozzi (2010) proposed that fine-grained pyrrhotite (<1μm) is identified through a Néel-like type of magnetic transition at ~35-32 K, named hereafter the P-transition and referred later as P-behaviour (Kars et al., 2011). Generally, the Néel transition is the signature of a mineral which is paramagnetic at room temperature and ferromagnetic below the Néel temperature.

We measured the IRM of claystone samples using a magnetic properties measurement system (MPMS) XL5 Ever Cool. The measurements were done on 400 mg of rock powder manually crushed and sealed in a gel capsule. Two types of results are extracted, corresponding graphically to the cooling of a RT-SIRM (room temperature IRM at saturation) and the warming of a LT-SIRM (low temperature IRM at saturation).

For the RT-SIRM, a 2.5 T field was applied at 300 K to impart the IRM and then switched off. The samples were cooled down to 10 K within an upward magnetic field of 5 μT (~1/10 of the Earth′s magnetic field) at about 5 K steps. This procedure allows the detection of magnetic transitions for temperatures <50K (Aubourg and Pozzi, 2010; Kars et al., 2011). For the LT-SIRM, we applied a magnetic field of 2.5T at 10K and monitored the remanence in a zero magnetic field. The samples were subsequently warmed back to 300 K at 10 K steps.

4. Results

4.1. Vitrinite reflectance (Ro) and Rock-Eval data

The vitrinite reflectance (Ro) and Rock-Eval data are presented in Table 1. The TOC values of the claystone samples collected away and within the contact aureole of magmatic intrusions are moderate to high, ranging between 1.02 to 10.25 wt%. The HI versus OI diagram indicates a predominance of type III "terrestrial" organic matter (OM) (Fig. 4a). The HI values are generally low (< 120 mg HC g^{-1} TOC). The OI shows a wide range of values that are spread between 5 to 73 mg CO_2 g^{-1} TOC. As a whole, the results of samples collected away from a sill or dyke intrusion are consistent with a normal burial trend. The latter is characterized by an initial decrease in OI values, and subsequent decrease of both OI and HI values indicating advanced diagenetic processes (Espitalié et al., 1986). The same trend in OI and HI values is observed for the samples collected within the thermal aureoles surrounding magmatic intrusions (Fig. 4a), hence indicating that the TOC, OI, and HI results did not identify the thermal aureoles.

Tmax and Ro also support a type III OM in the samples (Fig. 4b, where the grey area represents the range of values from Teichmüller and Durand (1983)). Immature type III OM is characterized by Ro ≤ 0.6-0.7% and Tmax≤ 435°C. Mature type III OM is in the oil window when 0.6-0.7%≤$Ro_{(oil\ window)}$ ≤1.3%, and 435°C≤$Tmax_{(oil\ window)}$ ≤470°C. Over-mature type III OM is characterized by Ro > 1.3% and Tmax≥ 470°C (Espitalié et al., 1985; Bordenave, 1993). For the samples away from the magmatic intrusions, the Tmax ranges from 422°C (G38) to 550°C (G48), and Ro varies from 0.37% (G46) to 1.57% (G48). These results show that most of the samples are immature to early mature, with one over-mature sample. The claystones identified as immature are from the proximal formations in the south and east of Nuussuaq (G51, G50, G49, G46), and to the eastern border of the sedimentary basin (G20, G31) (Fig. 1). These samples contain well-preserved plant debris and large vitrinite particles identified in their corresponding polished sections (Fig. 3), indicating that the reflectance values were confidently measured on in situ vitrinite particules. Therefore, the vitrinite reflectance values reported in Table 1 represent the maturity of the corresponding formation. The increasing values of Ro and Tmax from the proximal G46 to the distal G15 and G48 are probably the consequences of increasing burial depths to the western edge of the basin. In addition to the increased reflectivity, the vitrinite in the corresponding samples is also smaller in size (Fig. 3). G52 is sampled in the vicinity of the main border fault of the sedimentary basin and may have been altered by hydrothermal fluids.

Samples collected within a contact aureole show higher values of Ro (0.77-2%) and Tmax (442-604 °C) and are characteristic of mature to over-mature sediments (see Table 1), with the highest maturity closer to an intrusion. Sample G44, located between two dykes, shows a higher value of Ro (1.22%) and Tmax (446 °C), both characteristic of mature sediments. Sample G20, belongs to the same formation and same stratigraphic level of G44, but immature (Ro = 0.58% and Tmax = 432 °C). G33, from Qeqertarsuaq island indicates mature sediment with Ro value of 0.77% and Tmax value of 442 °C. G25 and G29 samples

collected in vicinity of magmatic intrusions are characteristic of mature to over-mature sediments (Table 1). We noticed an increasing thermal effect of magma intrusion from G25 (Ro of 0.89 and Tmax of 475°C) to G29 (Ro> 2% and Tmax of 604°C), corresponding to small vitrinite particles with an inhomogeneous reflectance pattern (Fig. 3).

Ro and Tmax values are sensitive to the duration and peak temperature of a heating episode, both of which can be estimated using the transfer functions of Sweeney and Burnham (1990). Values of Ro less than 0.32% and greater than 4% cannot be assigned to a specific maximum paleotemperature with confidence, and such values are given a maximum limit of 50°C and a minimum limit of 250°C. Here, organic matter of type III that experienced a peak burial temperature for 10 Ma and 100 Ma have corresponding oil windows in the ranges 110°C-160°C and 95°C-140°C, respectively. For background samples, the maximum paleotemperature derived from Ro is estimated to be between 55°C and 170°C when assuming heating rates of 1°C/Ma and cooling rates of 10°C/Ma (e.g., Green, 2003; Japsen et al., 2005) (Table 1). Therefore, the maturity (Tmax and Ro) as well as the maximum burial paleotemperature is well constrained for the background samples (Table 1). Since samples collected within a contact aureole are more sensitive to the peak temperature, the maximum paleotemperature is derived from Ro, and is estimated to be between 115°C to over >190°C, with the highest values closer to the intrusions.

4.2. Magnetic mineralogy

In this section and later discussion, we present the results from the magnetic experiments by separating the samples collected within and away from contact aureoles. The magnetic mineralogy is compared to the samples maturity as defined in Table 1.

4.2.1. Effect of burial depth

The magnetic mineralogy of the samples taken far from the thermal aureole of magma intrusions characterizes the background burial thermal history (G46, G50, G31, G51, G49, G20 G14, G19 G38, G15 and G48 in Table 2). The measured magnetic parameters are indicated in Table 2. The measured NRM intensity of the background claystone taken away from the thermal aureole has low values in the range of 10^{-3} to ~10^{-5}A m^{-1}. The magnetic susceptibility (χ) measured at room temperature shows values ranging between 21 μSI (for G19) and 547 μSI (for G51). Generally, the highest magnetic susceptibility (χ) is measured in the immature samples (Fig. 4c), and low values of magnetic susceptibility characterize the early mature to over mature samples. Furthermore, a clear magnetic susceptibility trend is noticed with a decreasing value from the proximal sediments to the distal sediments (Fig. 4c).

Measurements of the acquired IRM at room temperature indicate different patterns for immature and mature samples (Fig. 5). For the immature samples (e.g., G20, G46 and G31), only 70 to 90% of saturation is reached at 0.3T and specimens continue to acquire remanence at greater field strength (1.2 Tesla) (Fig. 5a), thus supporting the presence of high coercivity minerals such as hematite and/or goethite. On the other hand 90 to 95% of saturation is is reached at ~0.3 Tesla for the early mature and mature samples (G14, G19, G38, G15 and G48, Fig. 5b), thus indicating the presence of low coercivity minerals such as SD magnetite.

The representative immature (G46 G31 and G20) and early mature to mature samples (G19 and G15) are shown in figure 6. The maturity of these samples is characterized by an increase of Ro values (Fig. 6a), while the Tmax values indicate an immature stage. Such Tmax and Ro relationship illustrates the need of additional criterion to confidently constrain the maturity of claystones. The HT demagnetization of the IRM (Fig. 6b) outlines two distinct behaviors for the immature and the early mature/mature claystones: 1) a stepwise decrease of magnetisation up to 600°C with a slow slope-break around 350°C for the immature samples and: 2) a continuous decrease up 600°C with no slope-break around 350°C for the early mature samples (Fig. 6b).

For the immature samples, the composite IRM is dominated by low to medium coercivity (Fig. 6c). For sample G31, the drop of $IRM_{1.2Tesla}$ at 120°C corresponds to the Néel temperature of goethite (e.g., Özdemir and Dunlop, 1996). For the immature samples, a ~70% to ~90% drop of the IRM at 350°C (Fig. 6b) for all coercivities suggests a contribution to the remanence of iron sulfides such as greigite (Fe_3S_4) or monoclinic pyrrhotite (Fe_7S_8). Above 350°C, the steady decrease of the remanence of IRM up to 600°C indicates a contribution from magnetite (Fig.6b and c).

The RT-SIRM curve is characterized by an increase of remanence on cooling from 300 to 10K (G46, G31 and G20). This behaviour is indicative of goethite (α-FeOOH) or ultrafine-grained hematite (e.g., Maher et al., 2004). However, these samples are fully demagnetized at 600°C, well before the unblocking temperature of hematite (670°C), thus supporting the presence of high coercivity goethite. A marked drop of remanence in the slope for the LT-SIRM curve below 35/40K (Fig. 6d) could indicate the occurrence of ultra-fine superparamagnetic magnetic minerals in the immature samples (e.g., Guyodo et al., 2003). However, the absence of a Verwey transition at 120K for both RT-SIRM and LT-SIRM curves suggest the magnetite to be possibly oxidized or not stoichiometric (Özdemir et al., 2002).

The magnetic assemblage of the early mature samples is markedly different (Fig. 6). The HT demagnetisation of IRM for the G19 and G15 samples is continuous up to 600°C. The composite IRM in these two samples is dominated by low coercive minerals (Fig. 6c), supporting that the IRM is essentially

carried by magnetite. The medium and high coercive minerals for these two samples are quite similar in shape and values, thus indicating the contribution of other magnetic minerals to the remanence. For the RT-SIRM experiments, we did not notice any increase of remanence (Fig.6d) unlike the immature claystones. By contrast, we measured 1) a well-developed Verwey transition at 120K, indicative of stoichiometric magnetite, and 2) a P-behaviour that develops below 40K. The LT-SIRM curve shows a two-step decrease, with a break-in-slope at ~35K and ~120K, the latter corresponding to the Verwey transition of magnetite. The large drop of LT-SIRM below 35K could be the result of the contribution of fine-grained pyrrhotite (<1μm) and magnetite, which are in a superparamagnetic state at room temperature, and in ferromagnetic state at 10K.

The PM parameter, defined by Aubourg and Pozzi (2010), is used to estimate the contribution of magnetite over pyrrhotite, and is expressed as PM = (LT-SIRM10K−LT-SIRM35K) / (LT-SIRM10K). When PM is close to one, the pyrrhotite transition is well developed. When PM is near zero (i.e. small drop of LT-SRM), the magnetite overcomes the pyrrhotite contribution. Our results show an increase in PM values from the proximal and immature samples G20 (PM=0.55), G46 (PM = 0.73) and G31 (PM = 0.47) to the distal and mature samples G15 (PM=0.94) and G48 (PM=0.96) (Table 2).

4.2.2. Contact aureole samples

The magnetic mineralogy within contact aureoles was defined by samples G25, G29, G33, and G44. The measured NRM intensity of these samples has values ranging between 10^{-2} to 10^{-4}A m^{-1}, which is a magnitude higher than in the background samples (Table 2). The magnetic susceptibility measured at room temperature shows values ranging between 86 μSI and 164 μSI (Table 2). The saturation is reached between 0.3 and 0.5 Tesla for G25 and G29, thus indicating the presence of low coercivity minerals such as magnetite (Fig. 5c). For samples G44 and G33, the saturation is not reached, and both specimens continue to acquire remanence at greater field strength (1.2 Tesla) (Fig. 5c), indicating the presence of high coercivity minerals. Representative HT and LT demagnetisation curves are shown in figure 6 for G44, G25, and G29.

The HT demagnetisation of sample G44 shows a 82 % loss of the remanence at 350°C, thus supporting a contribution of iron sulfides. The steady decrease of IRM from 350°C up to 600°C indicates a contribution from magnetite (Fig. 7a). The composite IRM is dominated by low to medium coercivity typical for magnetite and possible minor contribution of iron sulfides to the remanence (Fig. 7b). The RT-SIRM curve is characterized by an increase of remanence when cooling from 300 to 10K. This behaviour is indicative of goethite. The LT-SIRM curve marked a drop in remanence until room temperature is reached (Fig. 7c), with a gentle break-in-slope in remanence below 35/40K. The absence of both a magnetic transition at 35K

when cooling down the RT-SIRM (Fig. 7c), and of a Verwey transition at 120K for both RT-SIRM and LT-SIRM curves suggest that magnetite is oxidized or is not stoichiometric.

The high temperature demagnetisation of sample G25 is characterised by a continuous decrease of IRM up to 600°C indicating the presence of magnetite. Similarly to G44, the composite IRM is dominated by low to medium coercivity phases (Fig. 7). In this case, a contribution of iron sulfides is supported by a 65 % loss in remanence at 350°C. The RT-SIRM and LT-SIRM curves are comparable to G44 sample. The HT demagnetisation of IRM for sample G29 outlines a stepwise decrease up to 600 °C with a gentle slope-break at around 350°C. The composite RT-IRM is dominated by the presence of low to medium coercive minerals, thus indicating that RT-IRM is essentially carried by magnetite and iron sulfides (greigite or pyrrhotite). A well-developed Verwey transition at 120K during the RT-SIRM and LT-SIRM experiments supports the presence of stoichiometric magnetite, and a P-behaviour that develops below 35/40K.

5. Discussion

The Svartenhuk-Disko Basin in the SE Baffin Bay volcanic margin is a case example where the effects of magmatic intrusions on country rocks are superimposed on burial and could be studied in detail. The thermal maturity analysis established for several samples in the area indicates a type-III immature to mature organic matter (Fig. 4). Generally, the immature samples are situated in the eastern and south-eastern parts of the basin where fluvial system and delta plain depositional environments dominate the sedimentary record (Fig. 1). The mature and over-mature samples characterize both the delta front and the pro-delta sedimentary successions in the western edge of the basin. Our maturity data are consistent with those reported in borehole GRO-3 (Fig. 8a), which reveal a depth-dependent increase in maturity with Ro values of 0.8% in the shallower sequences to 2.3% in the deepest units intersected in the well (Green, 2003). The maximum 40 to 50°C/km paleogeothermal gradient in the study area (Japsen et al., 2005) indicates a 1500 to 2000 m eroded sedimentary thickness in the area (Fig. 8a). Similarly to the maturity of the sediment, the maximum burial paleotemperatures increase westward. However, local increases in maturity reflect the thermal effects of magma intrusions, as for example in the Umiivik-1 well situated in the SE of the Svartenhuk-Halvø peninsula (Dam et al., 1998b) (see Figs. 1 and 2).

5.1. Burial effect on magnetic mineralogy

In the study area, the different magnetic assemblages are specific to proximal and distal sedimentary facies, and are consistent with increasing vitrinite reflectance values with maximum burial temperatures. Previous well-documented studies show that specific changes in magnetic mineral assemblages record an increase in burial depth (Aubourg and Pozzi, 2010; Aubourg et al., 2012; Kars et al., 2012; Blaise et al., 2014). The association of iron sulfide, goethite, and oxidized or non-stoichiometric single domain magnetite

characterizes the immature samples. Iron sulfides are produced during early to late diagenesis by bacterial alteration of the detrital magnetic minerals (e.g., Canfield and Berner, 1987), while the presence of pyrite and greigite are attributed to the dissolution of fine-grained magnetite (e.g., Roberts and Turner, 1993; Rowan and Roberts, 2006; 2009). Here, thermal demagnetisation of the samples indicates that ~70% to ~90% of the IRM is destroyed at 350°C. The lack of a magnetic transition at 35K (Fig.6d) indicates that pyrrhotite is absent (e.g., Dekkers et al., 1989). Therefore, our results show that the iron sulfide involved in the immature claystones stage is most likely greigite, diagnosed with both a Curie temperature close to 350°C and a lack of low temperature magnetic transition (e.g., Roberts et al., 2011) (Fig. 8b). Greigite is naturally stable only in specific chemical environments (sulfur-rich and reducing) and therefore is not necessary present in all sedimentary basins (e.g., Roberts et al., 2011). In addition, greigite is a typically unstable mineral, readily transforming into pyrite, and therefore its preservation through diagenetic and post-diagenetic processes tends to be rare (e.g., Blanchet et al., 2009). Below 282ºC, this mineral could be used as a valuable marker of peak temperatures reached in specific settings (Skinner et al., 1964).

The presence of goethite in our immature claystone samples (Fig. 8b) is rather unexpected because generally, goethite is commonly found in soils, eolian dusts, and laterites (e.g., Maher et al., 2004; Till et al., 2015). Chemical weathering onshore Greenland is typically limited to reworked moraine and glacial sediments along pro-glacial and non-glacial streams, and mostly selective to carbonate minerals (Deuerling et al., 2019). Therefore, the typical fresh exposures in Greenland where our samples were collected suggest that goethite was not formed as a result of chemical alteration during weathering. Furthermore, the presence of the greigite, formed in anoxic conditions, together with the absence of hematite, a classic marker of oxidizing environment, collectively do not support a weathering process for the formation of goethite. The presence of goethite in our immature claystone samples is interpreted to be either inherited or formed during burial. Inheritance of goethite is unlikely since bacterial activity and redox conditions within the first meters of sediments lead to the alteration of iron oxide, including magnetite, hematite and goethite (Rowan et al., 2009). Instead, we can safely propose here that the goethite is formed during burial. In addition, goethite is most likely nano-sized based on the absence of a break in the slope near 120°C, corresponding to the Néel temperature of goethite (Özdemir and Dunlop, 1996), and because goethite in our samples does not carry a significant portion of the natural remanence.

We identified a nano-sized pyrrhotite (< 1μm) and stoichiometric magnetite assemblage with a typical P-behavior in the early mature to mature argillaceous samples (Fig. 8b). Magnetite and fine-grained pyrrhotite are likely neoformed during burial as suggested by laboratory heating experiments of claystones at 95°C (Aubourg et al., 2008; Aubourg and Pozzi, 2010). The formation of micron-sized pyrrhotite in sediments is generally related to a temperature increase in anoxic conditions (Rochette, 1987).

Interestingly, we noticed a lower value of magnetic susceptibility at room temperature (Table 2) in the samples showing an increase in burial depth (G46, G50, G31, G51, G49, G20, G14, G19 G38, G15 and G48 see Fig. 4c and Tables 1 and 2) without any thermal influence of magma intrusion. This enigmatic decrease in magnetic susceptibility could be due to changes in mineralogy, concentration, and magnetic grain size distribution (e.g., Katz et al., 1998). Here, the HT demagnetization of the IRM shows the disappearance of the iron sulfide greigite (Fe_3S_4) and rise in magnetite (Fe_3O_4) following an increase in burial depth, from G46, G20, G38, G19, to G15 (Fig.9a). We observe a decrease in influence of iron sulfides on the magnetic signature at 350 °C, from ~80% (G46, G20 and G38) to 70% for G19 and 42% for G15. The RT-SIRM curves show a different trend between the immature samples and the early/to mature samples (Fig. 9b). For the LT-SIRM (for the increasing burial samples) (Figure 9c), we notice a decrease of remanence from 10K to 300K. The LT-SIRM shifted downward (more than two order of magnitude for G48) with increasing burial paleotemperatures. Aubourg and Pozzi (2010) and Kars et al., (2012) obtained similar results in heating experiments from 50°C to 130°C. The magnitude of this drop is larger for the deepest sample (high Ro and consequently high paleotemperature).

In the study area, magnetite was detected in almost all samples that experienced a burial temperature above 250 °C. Many studies reported also the occurrence of SD magnetite in rocks that experienced similar temperatures (e.g., Aubourg and Pozzi, 2010; Abdelmalak et al., 2012a; Blaise et al., 2014), and even wider temperature range from ~60 °C to >200 °C, or from the oil and beyond the gas windows (e.g., Cairanne et al., 2004; Aubourg et al., 2012; Kars et al., 2012). In addition, we also observed a P-behavior in our samples, indicating the occurrence of micron-sized pyrrhotite (<1 μm). Our results further show that temperatures did not exceed 200°C, with Ro values suggesting a maximum paleotemperature at around 170°C (G48) for background samples. The absence of a Besnus transition at 35 K in our samples indicates that> 1 μm pyrrhotite is absent (Aubourg et al., 2012), and that the paleotemperature in the study area did not exceed 350°C (Aubourg et al., 2019).

An increase in values of PM from 0.47 to 0.96 is noticed (Table 2) from the proximal samples (G46, G50, and G31, with the exception of G51) to the distal and deeper samples (G19, G15, and G48). The increase of PM values with increasing burial temperatures has been observed by Aubourg and Pozzi (2010) and Kars et al., (2012). Aubourg and Pozzi (2010) proposed a model of PM evolution with temperature characterized by a PM-up branch with an increase of PM value from ~50°C to a maximum value of ~90°C followed by PM down branch with a decrease of PM values from ~90°C to 250°C. Unfortunately, the limited number of samples in this study does not allow us to draw a clear evolution trend for the PM parameter.

5.2. Magma intrusion effect on magnetic mineralogy

With an additional thermal effect caused by magma intrusions, the magnetic signature of the samples became more complex. The vitrinite reflectance (Ro) of the proximal shallow marine claystone samples generally indicates that the sediments are immature, with values below 0.5%, except for the samples G33 and G44 collected within contact aureoles, with mature Ro values of 0.77% and 1.22%, respectively. The samples in more distal and deeper basinal settings G25 and G29 are mature to over-mature with respective Ro values of 0.89% and >2%, thus indicating an estimated maximum paleotemperature between 130°C to more than 190°C.

The HT-IRM demagnetization curves for samples G25, G44, and G29 show about 65 to 80% loss of magnetisation between room temperature and 350°C. The maximum unblocking temperature ranges between 500 and 600°C (Fig. 9d). These results indicate that the mineral assemblage in our samples is a mixture of iron sulfide (greigite) and magnetite. Sample G29 shows a Verwey transition at 120K indicative of stoichiometric magnetite, and a P-behaviour below 35/40K supporting the presence of micron-sized pyrrhotite (Fig. 9e).

The RT-SIRM curves show a similar trend for G33, G25, and G44 samples, but a different behavior is observed in sample G29 (Fig. 9e) with a decrease of the LT-SIRM from 10K to 300K (Fig. 9f). The increasing thermal effect could be the most likely explanation of the large drop of LT-SIRM (more than one order of magnitude) for sample G29 collected in the contact aureoles. Magnetite is interpreted to be the dominant magnetic mineral inside the contact aureole of the dyke/sill intrusions. The changes of magnetic signature at HT and LT could indicate a complex change in magnetite concentration in the heated sediments around an intrusion.

Similarly, Katz et al. (1998) showed that authigenic magnetite is the dominant magnetic phase in claystone within contact aureoles around intrusions. In addition, pyrrhotite may also be present closer to the intrusion contact where paleotemperatures were above 220°C, (Katz et al., 1998). In the East Greenland volcanic margin, Aubourg et al. (2014) reported the occurrence of >1μm pyrrhotite, characterized by a well-developed Besnus transition at 35 K, in sediments sampled in the thermal aureole of a magmatic intrusion. Therefore, the pyrrhotite detected in our samples is most likely related to contact metamorphism where paleotemperature exceeded 250 °C. In the Siberian Tunguska Basin, the Norilsk Nickel type of massive iron-sulfide deposits are composed of ca. 90% of pyrrothite (Malitch et al., 2014). These ore deposits are several tens of kilometers long and up to 45 m thick, andare located within the contact aureoles or inside the intrusions. In the outer Vøring Basin offshore mid-Norway, magnetotelluric data showed the presence of a highly conductive anomaly in heavily sill intruded sedimentary strata (depth ranging between 8–13 km and temperature between 250 and 400°C) (Corseri et al., 2017). These authors interpreted this geophysical anomaly to represent thick pyrrhotite-dominated ore bodies within the intrusion's contact metamorphic

aureoles. A study of the magnetic behaviour of natural pyrrhotite in the KTB ultra-deep borehole in Germany suggests that pyrrhotite overwhelmingly dominates at depths >8000 m or when in-situ temperatures exceed 230°C (Kontny et al., 2000). In our samples, the maximum temperature did not exceed 200°C, a conclusion based on a P-behavior indicative of micron-sized pyrrhotite (<1 μm) and elevated vitrinite reflectance value for G29 (Ro > 2%).

An important question relates to the origin of magnetite in the sediment samples near the magma intrusions, where chemical processes are either dominated by hydrothermal circulations or by heating. Hydrothermal fluids can cause alteration and subsequent precipitation of authigenic magnetite in a contact aureole (Ferry, 1991), or during alteration episodes (e.g., Jackson et al., 1988). In our samples, hydrothermal fluids had at best a negligible influence since the maturity of the organic matter are directly related to the thermal influence of the intrusion with changes in parameters following the normal heat diffusion distribution, as opposed to more random distribution that would be caused by fluid circulation with the contact aureole.

Despite the increase of temperatures, the iron sulfide greigite is still present in samples G25, G44, and G29 collected within the contact aureoles (Fig. 7), while samples affected only by burial processes have their greigite transformed into magnetite and fine-grained pyrrhotite (Figures 6 and 9a). Such observation has not previously been reported in lab simulations where the heating rates (1°C/mn) are very different from the natural heating rates, which are on the order of 5°C/My (e.g., Sweeney and Burnham, 1990). In addition, all of the experiments were performed at atmospheric pressure (0.1 MPa) (e.g., Kars et al., 2012), thus not simulating realistic burial conditions. Therefore, the differences between the lab experiments and our field samples on magnetic assemblage could be explained by the increase of the confining pressure (e.g., Bruijn et al., 2013).

5.3. Implications

The reconstruction of the thermal evolution of sedimentary basins is of key importance for evaluating their burial history and hydrocarbon potential (e.g., Suggate, 1998). Therefore, the thermal maturity of sediments should be measured using methods that collectively provide reliable results in both sedimentary and volcanic basins. The most common routine geothermometers include Rock-Eval pyrolysis (Tmax) and vitrinite reflectance (Ro) data, since both parameters allow inferring the maturity of organic matter in sedimentary sequences. Tmax and Ro values are sensitive to the type of organic matter in the sediments, and to the temperature evolution (e.g., Sweeney and Burnham, 1990). Therefore, these geothermometers are lithology-specific methods that are mostly applicable to organic rich sequences. In addition, our results show that Tmax and vitrinite reflectance are not reliable in the case of volcanic basins for confidently identifying contact aureoles. Similarly, Senger et al (2014) did not observe a clear trend in their Tmax data towards a dolerite intrusion on Svalbard. Instead, contact aureoles are defined by a combination of changes

that increase towards the intrusions, in particular with organic matter depletion, occurrence of metamorphic minerals, increase in carbon isotope fractionation, increase in fracturing, and drop in micro-porosity (Senger et al., 2014). These changes are attributed to be the result of devolatilization and decarbonation reactions by heating the country rocks (Aarnes et al., 2010; Aarnes et al., 2011; Senger et al., 2014).

The maturity parameters should also be independent from the type and content of organic matter in order to provide more reliable constraints on the basin's thermal history (Abdelmalak et al., 2012a; Blaise et al., 2014; Maré et al., 2014). To this effect, Aubourg and Pozzi (2010) proposed that magnetic mineral assemblage of claystones can be diagnostic of peak temperatures during burial. Furthermore, Aubourg et al. (2012) showed that the contours of a magnetic paragenesis define three successive magnetic windows in which greigite, magnetite and pyrrhotite occur with increasing burial depths. In this contribution, we suggest that the magnetic mineralogy of sediments can be used to confidently evaluate both the thermal maturity of sediments by burial (Fig. 8b) and by contact metamorphism. As opposed to the routine Tmax and vitrinite reflectance parameters, the magnetic mineralogy method does not appear to be influenced by the composition of sediments in organic matter, and furthermore seems to work in both volcanic and non-volcanic basin settings.

The use of the magnetic mineralogy method to estimate the thermal maturity of sedimentary sequences is relevant since volcanic basins are very common along conjugate margins that were formed by continental breakup and ocean opening. There, the (heavily intruded) pre-breakup sedimentary sequences and prolific source rock intervals may be over-mature in a contact aureole, and in the oil window just a few tens of meter away. This contributions shows that the magnetic mineralogy appears to be a good tool to confidently identify a metamorphic contact aureole in a borehole when the related magmatic intrusion have not been intersected in a borehole, or when the magmatic intrusion is bellow seismic resolution (i.e. vertical dyke or thin sill).

6. Conclusion

We have investigated the thermal effects of magmatic intrusions superimposed on normal burial processes on the magnetic mineral assemblages for samples collected in the Disko-Svartenhuk Basin situated in the central west Greenland. The magnetic properties of the samples form a trend following burial depth. The magnetic mineral assemblage consisting of greigite, goethite and oxidized or non-stoichiometric magnetite characterizes the immature samples, while stoichiometric magnetite and fine-grained pyrrhotite are typical for the early mature to mature samples. In addition, with increasing burial depth and subsequently paleotemperature, we noticed the disappearance of greigite following a rise in magnetite content.

In the metamorphic contact aureole of sill and dyke intrusions, magnetite is interpreted to be the dominant magnetic mineral when the temperatures did not exceed 200°C. In the proximal and shallow samples affected by magma intrusions, iron sulfides are still detected at temperature above 130°C. Intrusion-induced heating effect could be considered as analogue to burial heating, but some differences might exist when shallow sediments are intruded. Furthermore, the magnetic mineralogy is an effective geothermometer that appears to work in a wide range of basin settings since the method is independent of organic matter type and content. Therefore, this method can be used to build confidence on constraining the evolution of sedimentary basins by evaluating the thermal maturity of sediments given by the more standard Rock-Eval pyrolysis and the vitrinite reflectance methods.

Acknowledgements

Field investigation in West Greenland was supported by the Institut Polaire Français Paul Emile Victor (IPEV, program n° 290). We thank Copenhagen University for the use of the vessel *Porsild* during the expedition. Organic matter measurements were performed at ISTO (Institut des Sciences de la Terre d'Orléans) University of Orleans, France, under the supervision of Fatima Laggoun-Défarge. The MPMS XL5Ever Cool used in this study was financed by the Conseil Régional d'Ile-de-France (NºI-06-206/R), INSU-CNRS, IPGP and ANR. We would like to thank F. Lagroix for her help when running low-temperature experiments. We are thankful to Charles Aubourg, Laurent Geoffroy, Myriam Kars and Trond Helge Torsvik for their constructive discussions that improved the clarity of the early version of the manuscript. We would like to thank the reviewers Eric C. Ferré and William McCarthy, the editor, and associated editor Craig Magee for their helpful comments and guidance that improved the paper. We acknowledge the support from the Research Council of Norway through its Center of Excellence (CEED) (funding scheme, project 223272) and the Research Centre for Arctic Petroleum Exploration (ARCEx) which is funded by the Research Council of Norway (funding scheme, project 228107). There is no conflict of interest to declare.

Data availability Statement:

The data that support the findings of this study are available from the corresponding author upon reasonable request.

References

Aarnes, I., Svensen, H., Connolly, J.A.D., Podladchikov, Y.Y., 2010. How contact metamorphism can trigger global climate changes: Modeling gas generation around igneous sills in sedimentary basins. Geochimica et Cosmochimica Acta 74, 7179-7195.

Aarnes, I., Svensen, H., Polteau, S., Planke, S., 2011. Contact metamorphic devolatilization of shales in the Karoo Basin, South Africa, and the effects of multiple sill intrusions. Chemical Geology 281, 181-194.

Abdelmalak, M.M., 2010. Transition Spatio-temporelle entre rift sédimentaire et marge passive volcanique: l'exemple de la Baie de Baffin, Centre Ouest Groenland, (Spatio-temporal transition between a sedimentary basin to a volcanic passive margin: the Baffin Bay case example, Central West Greenland). Available at Université du Maine (France) onnline: http://cyberdoc.univ-lemans.fr/theses/2010/2010LEMA1030.pdf, Le Mans, p. 266.

Abdelmalak, M.M., Aubourg, C., Geoffroy, L., Laggoun-Deffarge, F., 2012a. A new oil-window indicator? The magnetic assemblage of claystones from the Baffin Bay volcanic margin. AAPG Bulletin 96, 205-215.

Abdelmalak, M.M., Geoffroy, L., Angelier, J., Bonin, B., Callot, J.P., Gélard, J.P., Aubourg, C., 2012b. Stress fields acting during lithosphere breakup above a melting mantle: A case example in West Greenland. Tectonophysics 581, 132-143.

Abdelmalak, M.M., Planke, S., Polteau, S., Hatz, E.H., Faleide, J.I., Tegner, C., Jerram, D.A., Millett, J.M., Myklebust, R., 2019. Breakup volcanism and plate tectonics in the NW Atlantic. Tectonophysics.

Aubourg, C., Jackson, M., Ducoux, M., Mansour, M., 2019. Magnetite-out and pyrrhotite-in temperatures in shales and slates. Terra Nova 31, 534-539.

Aubourg, C., Pozzi, J.-P., 2010. Toward a new < 250 °C pyrrhotite-magnetite geothermometer for claystones. Earth and Planetary Science Letters 294, 47-57.

Aubourg, C., Pozzi, J.-P., Kars, M., 2012. Burial, claystones remagnetization and some consequences for magnetostratigraphy. Geological Society, London, Special Publications 371, 181-188.

Aubourg, C., Pozzi, J.P., Janots, D., Sahraoui, L., 2008. Imprinting chemical remanent magnetization in claystones at 95 °C. Earth and Planetary Science Letters 272, 172-180.

Aubourg, C., Techer, I., Geoffroy, L., Clauer, N., Baudin, F., 2014. Detecting the thermal aureole of a magmatic intrusion in immature to mature sediments: a case study in the East Greenland Basin (73°N). Geophysical Journal International 196, 160-174.

Banerjee, S., Elmore, R.D., Engel, M.H., 1997. Chemical remagnetization and burial diagenesis: Testing the hypothesis in the Pennsylvanian Belden Formation, Colorado. Journal of Geophysical Research: Solid Earth 102, 24825-24842.

Bishop, A.N., Abbott, G.D., 1995. Vitrinite reflectance and molecular geochemistry of Jurassic sediments: the influence of heating by Tertiary dykes (northwest Scotland). Organic Geochemistry 22, 165-177.

Blaise, T., Barbarand, J., Kars, M., Ploquin, F., Aubourg, C., Brigaud, B., Cathelineau, M., El Albani, A., Gautheron, C., Izart, A., Janots, D., Michels, R., Pagel, M., Pozzi, J.-P., Boiron, M.-C., Landrein, P., 2014. Reconstruction of low temperature (<100 °C) burial in sedimentary basins: A comparison of geothermometer in the intracontinental Paris Basin. Marine and Petroleum Geology 53, 71-87.

Blanchet, C.L., Thouveny, N., Vidal, L., 2009. Formation and preservation of greigite (Fe3S4) in sediments from the Santa Barbara Basin: Implications for paleoenvironmental changes during the past 35 ka. Paleoceanography 24.

Bojesen-Koefoed, J.A., Christiansen, F.G., Nytoft, H.P., Dalhoff, F., 1997. Organic geochemistry and thermal maturity of sediments in the GRO#3 well, Nuussuaq, West Greenland. Danm. Grønl. Geol. Unders. Rap 43, 18.

Bonow, J.M., Japsen, P., Lidmar-Bergstrom, K., Chalmers, J.A., Pedersen, A.K., 2006. Cenozoic uplift of Nuussuaq and Disko, West Greenland-elevated erosion surfaces as uplift markers of a passive margin. Geomorphology 80, 325-337.

Bordenave, M.L., 1993. Applied petroleum geochemistery, Technip ed. Technip, Paris.

Brothers, L.A., Engel, M.H., Elmore, R.D., 1996. The late diagenetic conversion of pyrite to magnetite by organically complexed ferric iron. Chemical Geology 130, 1-14.

Bruijn, R.H.C., Almqvist, B.S.G., Hirt, A.M., Benson, P.M., 2013. Decoupling of paramagnetic and ferrimagnetic AMS development during the experimental chemical compaction of illite shale powder. Geophysical Journal International 192, 975-985.

Burnham, A.K., Sweeney, J., J.,, 1989. A chemical kinetic model of vitrinite maturation and reflectance. Geochomica et Cosmochimica Acta 53, 2649-2657.

Cairanne, G., Aubourg, C., Pozzi, J.P., Moreau, M.G., Decamps, T., Marolleau, G., 2004. Laboratory chemical remanent magnetization in a natural claystone: a record of two magnetic polarities. Geophysical Journal International 159, 909-916.

Canfield, D.E., Berner, R.A., 1987. Dissolution and pyritization of magnetite in anoxie marine sediments. Geochimica et Cosmochimica Acta 51, 645-659.

Chalmers, J.A., Pulvertaft, T.C.R., 2001. Development of the continental margins of the Labrador Sea: a review, in: Wilson, R.C.L., Whitmarsh, R.B., Taylor, B., Froitzheim, N. (Eds.), Non-volcanic Rifting of Continental Margins: a Comparison of Evidences from Land and Sea. Geological Society Special Publication, London, pp. 77-105.

Corseri, R., Senger, K., Selway, K., Abdelmalak, M.M., Planke, S., Jerram, D., 2017. Magnetotelluric evidence for massive sulphide mineralization in intruded sediments of the outer Vøring Basin, mid-Norway. Tectonophysics 706-707, 196-205.

Dam, G., 2002. Sedimentology of magmatically and structurally controlled outburst valleys along rifted volcanic margins: exemples from the Nuussuaq Basin, West Greenland. Sedimentology 49, pp 505-532.

Dam, G., Larsen, M., Sonderholm, M., 1998a. Sedimentary response to mantle plumes: implication from Palaeocene onshore successions, West and East Greenland. Geology 26, 207-210.

Dam, G., Nohr-Hansen, H., Christiansen, F.G., Bosjesen-Kofoed, J.A., Laier, T., 1998b. The oldest marine Cretaceous sediments in west Greenland (Umiivik-1borehole)- record of the Cenomanian-Turonian Anoxic Event? geology of greenland survey bulletin 180, 128-137.

Dam, G., Nohr-Hansen, H., Pedersen, G.K., Sonderholm, M., 2000. Sedimentary and structural evidence of a new early Campanian rift phase in the Nuussuaq Basin, West Greenland. Cretaceous Research 21, 127-154.

Dam, G., Pedersen, G.K., Sonderholm, M., Midtgaard, H., H.,, Larsen, L.M., Nohr-Hansen, H., Pedersen, A.K., 2009. Lithostratigraphy of the Cretaceous-Pleocene Nuussuaq Group, Nuussuaq Bsin, West Greenland. geological survey of Denmark and gdeenland Bulletin 19, 171.

Dekkers, M.J., 1989. Magnetic properties of natural goethite- I grain size dependence of somme low - and high-field related rock magnetic parameters measured at room temperature. Geophysical Journal 97, 323-340.

Dekkers, M.J., Mattéi, J.L., Fillion, G., Rochette, P., 1989. Grain-size dependence of the magnetic behavior of pyrrhotite during its low-temperature transition at 34 K. Geophysical Research Letters 16, 855-858.

Deuerling, K.M., Martin, J.B., Martin, E.E., Abermann, J., Myreng, S.M., Petersen, D., Rennermalm, Å.K., 2019. Chemical weathering across the western foreland of the Greenland Ice Sheet. Geochimica et Cosmochimica Acta 245, 426-440.

Dunlop, D.J., 1995. Magnetism in rocks. Journal of Geophysical Research 100, 2161-2174.

Dunlop, D.J., Özdemir, Ö., 1997. Rock Magnetism, Fundamentals and Frontiers. Cambridge University Press, Cambridge.

Elmore, D.R., Lee-Egger Foucher, J., Evans, M., Lewchuk, M., Cox, E., 2006. Remagnetization of the Tonoloway Formation and the Helderberg Group in the Central Appalachians: testing the origin of syntilting magnetizations. Geophysical Journal International 166, 1062-1076.

Elmore, R.D., Engel, M.H., Crawford, L., Nick, K., Imbus, S., Sofer, Z., 1987. Evidence for a relationship between hydrocarbons and authigenic magnetite. Nature 325, 428-430.

Espitalié, J., Deroo, G., Marquis, F., 1985. La pyrolyse Rock-Eval et ses applications, part I. Revue Institut Français de Pétrole 10, 563-578.

Espitalié, J., Deroo, G., Marquis, F., 1986. La pyrolyse Rock-Eval et ses applications, Part III. Revue Institut Français de Pétrole 41, 467-481.

Ferry, J.M., 1991. Dehydration and decarbonation reactions as a record of fluid infiltration. Reviews in Mineralogy and Geochemistry 26, 351-393.

Geoffroy, L., 2001. The structure of volcanic margins: some problematics from the North-Atlantic/ Labrador-Baffin System. Marine and Petroleum Geology 18, 463-469.

Gillett, S.L., 2003. Paleomagnetism of the Notch Peak contact metamorphic aureole, revisited: pyrrhotite from magnetite + pyrite under submetamorphic conditions. journal of geophysical research 108, 2446.

Green, P.F., 2003. thermal history reconstruction in the Ataa-1, Gane-1, Gant-1, Gro-3 and Umivik-1 boreholes, onshore west Greenland, based on AFTA, vitrinite reflectence and apatite (U-Th)/He dating. A report for GEUS by Geotrack International Pty Ltd. Geotrack report 883, 1-250.

Green, P.F., Japsen, P., Chalmers, J.A., Bonow, J.M., 2011. Thermochronology, erosion surfaces and missing section in West Greenland. Journal of the Geological Society 168, 817-830.

Guyodo, Y., Mostrom, A., Penn, R.L., Banerjee, S.K., 2003. From nanodots to nanorods: oriented aggregation and magnetic evolution of nanocrystalline goethite. Geophysical Research Letters 30, 1512.

Haxby, W.F., Turcotte, D.L., Bird, J.M., 1976. Thermal and mechanical evolution of the Michigan Basin. Tectonophysics 36, 57-75.

ICCP, 1971. International committee for Coal Pertology. International Handbook of Coal Petrograpgy, 2nd ed. CNRS, Paris.

Jackson, M., McCabe, C., Ballard, M.M., Van der Voo, R., 1988. Magnetite authigenesis and diagenetic paleotemperatures across the northern Appalachian basin. Geology 16, 592-595.

Japsen, P., Bonow, J.M., Green, P.F., Chalmers, J.A., Lidmar-Bergstrom, K., 2006. Elevated, passive continental margins: Long-term highs or Neogene uplifts? New evidence from West Greenland. Earth and Planetary Science Letters 248, 330-339.

Japsen, P., Bonow, J.M., Green, P.F., Chalmers, J.A., Lidmar-Bergström, K., 2009. Formation, Uplift and dissection of planation surface at passive continental margins - a new approach. Earth Surface Processes and Landforms 34, 683-699.

Japsen, P., Green, P.F., Bonow, J.M., Rasmussen, E.S., Chalmers, J.A., Kjennerud, T., 2010. Episodic uplift and exhumation along North Atlantic passive margins: implications for hydrocarbon prospectivity. Geological Society, London, Petroleum Geology Conference series 7, 979-1004.

Japsen, P., Green, P.F., Chalmers, J.A., 2005. Separation of Palaeogene and Neogene uplift on Nuussuaq, West Greenland. journal of Geological Society, London 162, 299-314.

Just, J., Kontny, A., De Wall, H., Hirt, A.M., Martín-Hernández, F., 2004. Development of magnetic fabrics during hydrothermal alteration in the Soultz-sous-Forêts granite from the EPS-1 borehole, Upper Rhine Graben. Geological Society, London, Special Publications 238, 509-526.

Kars, M., Aubourg, C., Pozzi, J.-P., 2011. Low temperature magnetic behaviour near 35 K in unmetamorphosed claystones. Geophysical Journal International 186, 1029-1035.

Kars, M., Aubourg, C., Pozzi, J.-P., Janots, D., 2012. Continuous production of nanosized magnetite through low grade burial. Geochemistry, Geophysics, Geosystems 13, 12.

Katz, B., Elmore, R.D., Cogoini, M., Engel, M.H., Ferry, S., 2000. Associations between burial diagenesis of smectite, chemical remagnetization, and magnetite authigenesis in the Vocontian trough, SE France. Journal of Geophysical Research: Solid Earth 105, 851-868.

Katz, B., Elmore, R.D., Engel, M.H., 1998. Authigenesis of magnetite in organic-rich sediment next to a dike: implications for thermoviscous and chemical remagnetizations. Earth and Planetary Science Letters 163, 221-234.

Kontny, A., de Wall, H., Sharp, T.G., Pósfai, M., 2000. Mineralogy and magnetic behavior of pyrrhotite from a 260 °C section at the KTB drilling site, Germany. American Mineralogist 85, 1416-1427.

Lafargue, E., Marquis, F., Poillot, D., 1998. Rock-Eval 6 application in hydrocarbon exploration, production, and soil contamination studies. Revue Institut Français de Pétrole 56 (4), 421-437.

Lo, H.B., 1992. Identification of indigenous vitrinites for improved thermal maturity evaluation. Organic Geochemistry 18 (3), 359-364.

Lowrie, W., 1990. Identification of ferromagnetic minerals in a rock by coercivity and unblocking temperature properties. Geophysical Research Letters 17, 159-162.

Maher, B.A., Karloukovski, V.V., Mutch, T.J., 2004. High-field remanence properties of synthetic and natural submicrometre haematites and goethites: significance for environmental contexts. earth and planetary science letters 226, 491-505.

Malitch, K.N., Latypov, R.M., Badanina, I.Y., Sluzhenikin, S.F., 2014. Insights into ore genesis of Ni-Cu-PGE sulfide deposits of the Noril'sk Province (Russia): Evidence from copper and sulfur isotopes. Lithos 204, 172-187.

Maré, L.P., De Kock, M.O., Cairncross, B., Mouri, H., 2014. Application of magnetic geothermometers in sedimentary basins: an example from the western Karoo basin, South Africa. South African Journal of Geology 117, 1-14.

McCabe, C., Jackson, M., Saffer, B., 1989. Regional patterns of magnetite authigenesis in the Appalachian Basin: Implications for the mechanism of Late Paleozoic remagnetization. Journal of Geophysical Research: Solid Earth 94, 10429-10443.

Moreau, M.G., Ader, M., Enkin, R.J., 2005. The magnetization of clay-rich rocks in sedimentary basins: low-temperature experimental formation of magnetic carriers in natural samples. Earth and Planetary Science Letters 230, 193-210.

Muxworthy, A.R., McClelland, E., 2000. Review of the low-temperature magnetic properties of magnetite from a rock magnetic perspective. Geophysical Journal International 140, 101-114.

Palumbo, F., Main, I.G., Zito, G., 1999. The thermal evolution of sedimentary basins and its effect on the maturation of hydrocarbons. Geophysical Journal International 139, 248-260.

Petronis, M.S., O'Driscoll, B., Lindline, J., 2011. Late stage oxide growth associated with hydrothermal alteration of the Western Granite, Isle of Rum, NW Scotland. Geochemistry, Geophysics, Geosystems 12.

Piasecki, S., Larsen, L.M., Pedersen, A.K., Pedersen, G.K., 1992. Palynostratigraphy of the Lower Tertiary volcanics and marine clastic sediments in the southern part of the West Greenland Basin: implication fortiming and duration of the volcanism. Rapport Groenlands geologiske Undersogelse 154, 13-31.

Roberts, A.P., 2015. Magnetic mineral diagenesis. Earth-Science Reviews 151, 1-47.

Roberts, A.P., Chang, L., Rowan, C.J., Horng, C.-S., Florindo, F., 2011. Magnetic properties of sedimentary greigite (Fe3S4): An update. Reviews of Geophysics 49, RG1002.

Roberts, A.P., Turner, G.M., 1993. Diagenetic formation of ferrimagnetic iron sulphide minerals in rapidly deposited marine sediments, South Island, New Zealand. earth and planetary science letters 115, 257-273.

Roberts, A.P., Weaver, R., 2005. Multiple mechanisms of remagnetization involving sedimentary greigite (Fe3S4). Earth and Planetary Science Letters 231, 263-277.

Rochette, P., 1987. Magnetic susceptibility of the rock matrix related to magnetic fabric studies. Journal of Structural Geology 9, 1015-1020.

Rochette, P., Fillion, G., Mattéi, J.-L., Dekkers, M.J., 1990. Magnetic transition at 30–40 K in pyrrhotite: insight into a widespread occurrence of this mineral in rocks. earth and planetary science letters 98, 319-328.

Rowan, C.J., Roberts, A.P., 2006. Magnetite dissolution, diachronous greigite formation, and secondary magnetizations from pyrite oxidation: Unravelling complex magnetizations in Neogene marine sediments from New Zealand. Earth and Planetary Science Letters 241, 119-137.

Rowan, C.J., Roberts, A.P., Broadbent, T., 2009. Reductive diagenesis, magnetite dissolution, greigite growth and paleomagnetic smoothing in marine sediments: A new view. Earth and Planetary Science Letters 277, 223-235.

Senger, K., Planke, S., Polteau, S., Ogata, K., Svensen, H., 2014. Sill emplacement and contact metamorphism in a siliciclastic reservoir on Svalbard, Arctic Norway. Norsk Geologisk Tidsskrift 94, 155-169.

Skinner, B.J., Erd, R.C., Grimaldi, F.S., 1964. Greigite, the thio-spinel of iron; a new mineral. American Mineralogist 49, 543-555.

Suggate, R.P., 1998. Relations between depth of burial, Vitinite reflectance and geothermal gradient. Journal of Petroleum Geology 21, 5-32.

Sweeney, J., J.,, Burnham, A.K., 1990. Evaluation of a simple Model of Vitrinite Reflectance Based on Chemical Kinetics. The American Association of Petroleum Geologists 74, 1559-1570.

Teichmüller, M., Durand, B., 1983. Fluorescence microscopal rank studies on liptinites and vitrinites in peat and coals and comparison with result of Rock-Eval pyrolysis. International Journal of Coal Geology 2, 197-230.

Till, J.L., Guyodo, Y., Lagroix, F., Morin, G., Ona-Nguema, G., 2015. Goethite as a potential source of magnetic nanoparticles in sediments. Geology 43, 75-78.

van Velzen, A.J., Zijderveld, J.D.A., 1992. A method to study alterations of magnetic minerals during thermal demagnetization applied to a fine-grained marine marl (Trubi formation, Sicily). Geophysical Journal International 110, 79-90.

Walz, F., 2002. The Verwey transition - a topical review. Journal of Physics: Condensed Matter 14, R285.

Welte, D., Yukler, M., 1981. Petroleum origin and accumulation in basin evolution - A quantitative model. American Association of Petroleum Geologists Bulletin 65.

Özdemir, Ö., Dunlop, D.J., 1996. Thermoremanence and Néel temperature of goethite. Geophysical Research Letters 23, 921-924.

Özdemir, Ö., Dunlop, D.J., Moskowitz, B.M., 2002. Changes in remanence, coercivity and domain state at low temperature in magnetite. Earth and Planetary Science Letters 194, 343-358.

Figures caption

Figure 1. (a) Simplified geological map of the Disko-Svartenhuk Basin (based on the Geological Survey of Denmark and Greenland maps and Chalmers et al., 1999). The locations of the 16 claystones samples are indicated. (b) Paleogeographic reconstruction of the studied area during the Cretaceous time (Abdelmalak, 2010). The proximal sedimentary facies are situated to the south and eastern part of the studied area and consist mainly of the fluvial channel and the delta plain deposits. The distal sedimentary facies are located to the west and northwestern part of the studied area and consist mainly of the delta front and the prodelta deposits. Arrows indicate the direction of the sediment transport.

Figure 2. Lithostratigraphic position of the samples in the Itsako and Qeqertarsuaq islands (Dam et al., 2009) shown in log and in the AB cross section. The location of the Umiviik-1 borehole is indicated. The proximal samples are represented by G20, G31, G33 and G44; the distal samples are represented by G25, G29 and G38. Samples G44, G33, G25 and G29 are comprised within the thermal aureole effect of magma intrusions.

Figure 3. Microphotographs of dispersed organic matter in samples from this study. Immature samples contain well-preserved plant debris (G31, G46 and G50), and large and angular vitrinite particles (G46, G49 and G31) with pyrite and framboid pyrite particles. Mature samples contain smaller virtinite particles (G15, G48 and G38). Microphotographs of samples G29, G25 and G44 show dispersed organic matter in samples collected within the metamorphic contact aureoles. Vitrinite (1) is autochthonous, and vitrinite (2) is reworked and allochthonous.

Figure 4. (a) Hydrogen index (HI) versus Oxygen index (OI) diagram. The burial trend and the different types of organic matter (OM as marine-derived type II and the higher plants derived type III) are indicated. (b) Tmax (°C) versus Vitrinite reflectance Ro (%) diagram. The grey shaded area corresponds to the Ro/Tmax correlation for type III OM after Teichmüller and Duran (1983). The oil window is indicated by a black box. The samples affected by thermal aureole are represented in red. (c) Dimensionless magnetic susceptibility χ (μSI) versus Vitrinite reflectance Ro (%) diagram.

Figure 5. Isothermal Remanent Magnetization (IRM) acquisition curves for the: (a) immature samples, (b) early mature to mature samples and (c) mature samples taken in the thermal aureole of magma intrusions. We plot the normalized IRM to the value of IRM at 1.2T.

Figure 6. Representative results of immature claystones (G46 G31 and G2) and early mature (G19 and G15). (a) Histogram of the reflectance of vitrinite (Ro%). The Tmax from Rock-Eval analysis are indicated. (b) Normalized demagnetization of isothermal remanent magnetization (IRM). (c) The high temperature

magnetic curves from warming of a composite IRM acquired at room temperature following Lowrie's (1990) protocol. (d) The low temperature magnetic curves from RT-SIRM demagnetization curve on cooling and LT-SIRM demagnetization curves (10K-300K) on warming. We normalized RT-SIRM and LT-SIRM to the value of RT-SIRM at 300 K and LT-SIRM at 10 K respectively.

Figure 7. Magnetic signature for samples taken in the thermal aureole of magma intrusion. (a) Normalized high temperature demagnetization of isothermal remanent magnetization (IRM). (b) High temperature magnetic curves from warming of a composite IRM. (c) Low temperature magnetic curves from RT-SIRM demagnetization curve on cooling and LT-SIRM demagnetization curves (10K-300K) on warming. The Tmax values from Rock-Eval analysis are indicated.

Figure 8. (a) paleotempereature and vitrinite reflectance data of the Gro-3 well (See Fig. 1 for location) situated west of Nuussuaq based on the Christiansen et al. (1999) well data assuming a geothermal gradient ranging between 40 and 50 °C/km (Japsen et al., 2005). The removed section is indicated and the depth is corrected. (b) Model showing the formation of magnetic mineral as a function of organic matter maturity and temperature using samples of this study.

Figure 9. (a) Normalized high temperature demagnetization of isothermal remanent magnetization (IRM) with increasing burial. (b) RT-SIRM evolution of samples with increasing burial. (c) LT-SIRM evolution of samples with increasing burial. (d) Normalized high temperature demagnetization of IRM with increasing effect of magma intrusion. (e) RT-SIRM evolution of samples with increasing magmatic thermal effect. (f) LT-SIRM evolution of samples with increasing thermal effect from magma intrusions. The paleotemperature (on c and f) and the PM parameter (on b and e) are indicated.

Tables caption

Table 1: Sample location, Rock-Eval, Vitrinite reflectance results, and estimated paleotemperatures.

Table 2: Magnetic data of the claystone samples.

Table 1:

Sample	Sedimentary facies		Location			Rock-Eval				Vitrinite			Paleotemperature (°C)	Maturity
			Lat (° N)	Long (° W)	Elevation (m)	Tmax (°C)	TOC	HI	OI	Ro (%)	±std	N		
G46	Proximal	Increasing burial depth	70° 37.52'	52° 20.94'	203	429	4.01	43	73	0.37	0.12	91	55	immature
G50	Proximal		70° 18. 02'	52° 54.74'	64	433	6.38	33	53	0.46	0.09	100	64	immature
G31	Proximal		71° 43.81'	53° 46.97'	134	429	2.19	44	54	0.47	0.07	100	67	immature
G51	Proximal		70° 03.27'	52° 17.18'	0	433	3.71	69	25	0.49	0.10	100	71	immature
G49	Proximal		70° 22.35'	53° 35.00'	0	431	9.24	63	23	0.48	0.08	100	69	immature
G20	Proximal		71° 10.02'	52° 29.22'	0	432	2.13	32	56	0.58	0.10	100	89	immature
G14	Proximal		70° 45.87'	53° 03.39'	212	432	6.52	83	15	0.59	0.09	100	90	immature
G19	Distal		70° 44.43'	52° 44.83'	0	428	3.49	119	12	0.6	0.11	100	92	mature
G38	Distal		71° 33.97'	53° 55.20’	175	422	7.09	32	33	0.62	0.13	100	96	mature
G15	Distal		70° 45.16'	53° 22.35'	55	430	4.38	79	8	0.91	0.15	100	130	mature
G48	Distal		70° 47.28'	53° 45.62’	0	550	6.55	22	5	1.57	0.14	60	170	overmature
G33	Proximal	Intrusion effect	71° 37.06'	53° 26.52’	0	442	2.75	89	18	0.77	0.08	84	115	mature
G25	Distal		71° 42.77'	53° 47.09'	698	475	1.02	7	38	0.89	0.25	100	130	mature
G44	Proximal		71° 09.45'	52° 56.92'	0	446	2.15	64	13	1.22	0.26	100	155	mature
G29	Distal		71° 38.22'	53° 47.30'	0	604	3.18	3	11	>2		40	>190	overmature
G52	Proximal	Alteration	70° 04.37’	52° 10.16'	447	436	10.75	122	27	0.68	0.09	100	105	mature

Tmax: temperature at maximum release of hydrocarbons; TOC: Total Organic content (wt%); HI: Hydrogen Index (HI, mg HC/g TOC); OI: Oxygen Index (OI, mg CO_2/g TOC); Ro: vitrinite reflectance; std: standard deviation; N: number of measurements per sample.

Table 2

Sample	Mass (g)	χ (μ)	300K RT-NRM A/m	300K RT-IRM A/m	Per cent 350° C	300K RT-SIRM mAm²/Kg	10K LT-SIRM mAm²/Kg	35K LT-SIRM mAm²/Kg	PM
G46	4.38	215	8.84E-04	1.76E-01	83	553	1.60E-02	4.37E-03	0.73
G50	5.6	142	7.45E-04	1.05E-02	-	43	1.32E-03	3.45E-04	0.74
G31	4.38	106	1.24E-03	6.99E-03	93	74	7.01E-04	3.74E-04	0.47
G51	4.62	547	1.17E-03	6.23E-02	98	80	1.47E-02	8.90E-04	0.94
G49	4.6	107	1.07E-03	4.14E-02	52	34	2.73E-03	1.06E-04	0.96
G20	6.19	151	5.88E-04	3.91E-02	89	14	1.93E-03	8.66E-04	0.55
G14	5.66	47	6.80E-04	3.58E-03	53	14	3.49E-04	3.84E-05	0.89
G19	6.09	21	7.12E-04	4.60E-03	70	21	4.95E-04	5.50E-05	0.89
G38	2.85	54	1.12E-03	1.91E-02	80	80	1.03E-03	5.45E-04	0.47
G15	9.8	61	1.30E-03	2.44E-02	42	41	1.80E-03	1.04E-04	0.94
G48	2.94	43	3.37E-04	4.95E-03	74	13	1.65E-03	6.57E-05	0.96
G33	2.13	98	1.22E-03	7.61E-03	-	55	9.53E-04	2.66E-04	0.72
G25	7.08	164	1.44E-02	1.32E-02	65	51	3.86E-03	3.18E-04	0.92
G44	3.53	159	7.19E-04	2.40E-02	82	68	1.71E-03	5.66E-04	0.67
G29	4.57	86	1.26E-03	9.00E-03	78	20	1.36E-03	7.81E-05	0.94

G52	2.81	97	7.36E-04	9.67E-03	85	253	1.77E-03	6.43E-04	0.64

χ: magnetic susceptibility (dimensionless); RT-NRM: room temperature natural remanent magnetization; RT-IRM: room temperature isothermal remanent magnetization; Per cent 350° C: drop of magnetisation at 350° C; RT-SIRM: room temperature IRM at saturation; PM=(LT-SIRM10K−LT-SIRM35K) /LT-SIRM10K (Aubourg and Pozzi, 2010).

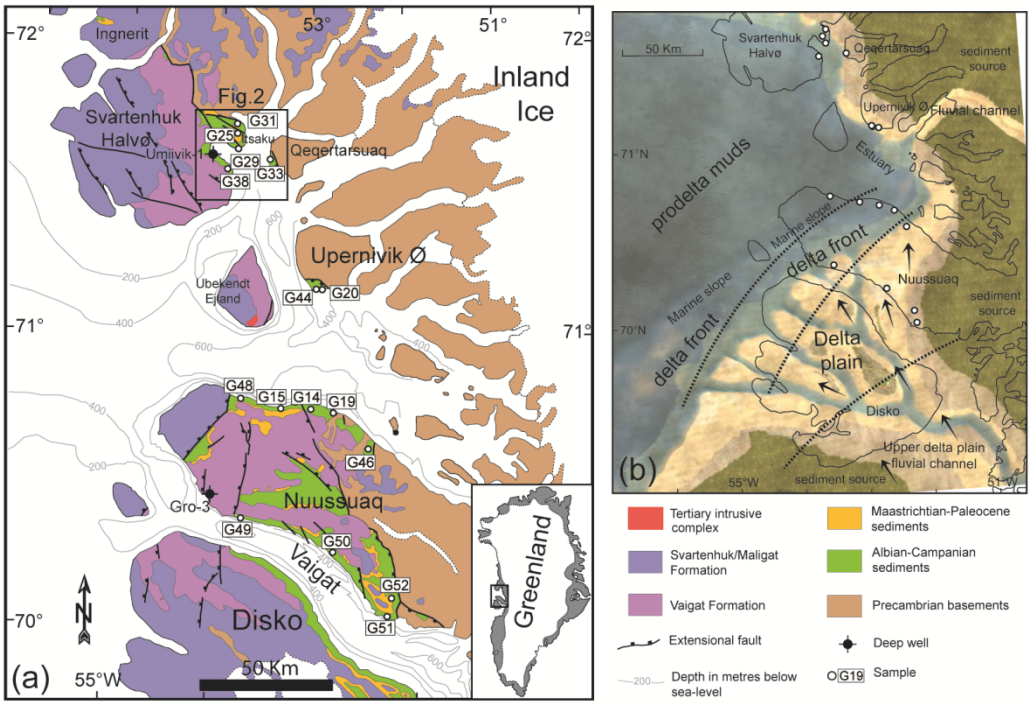

bre_12439_f1.tif

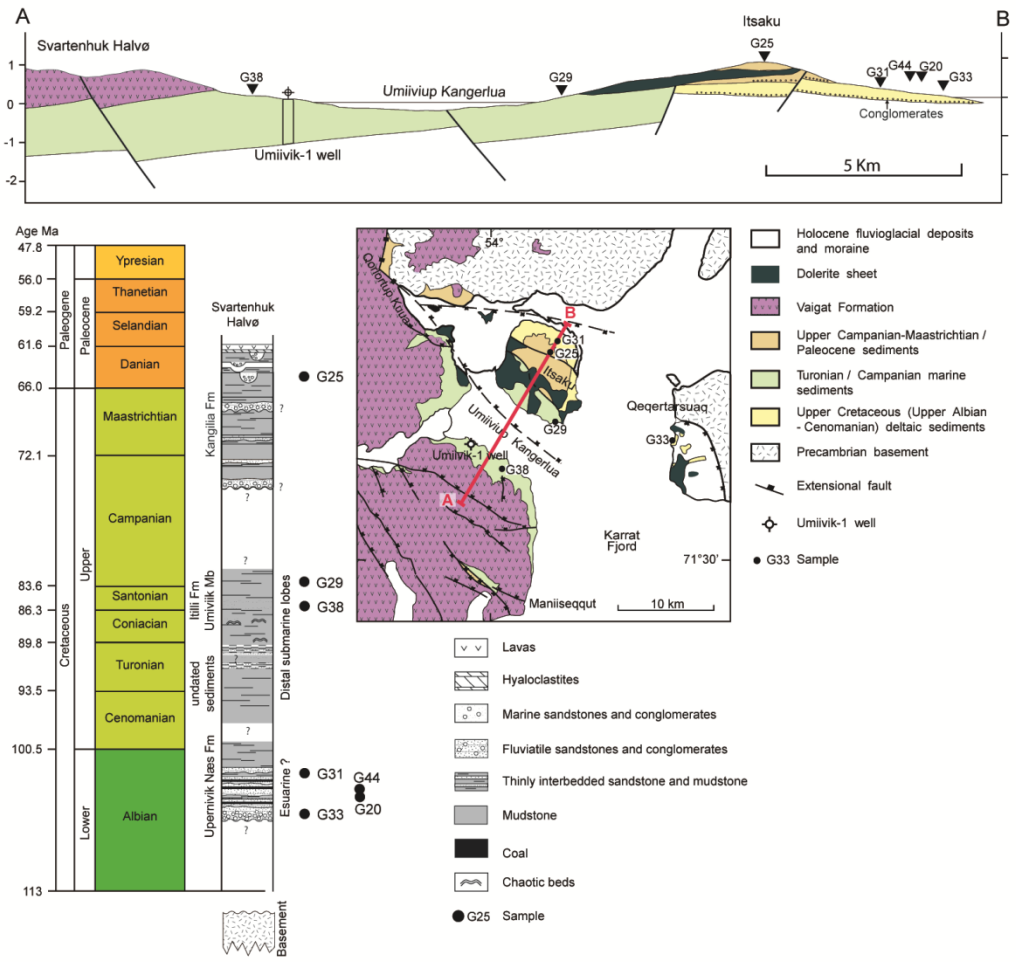

bre_12439_f2.tif

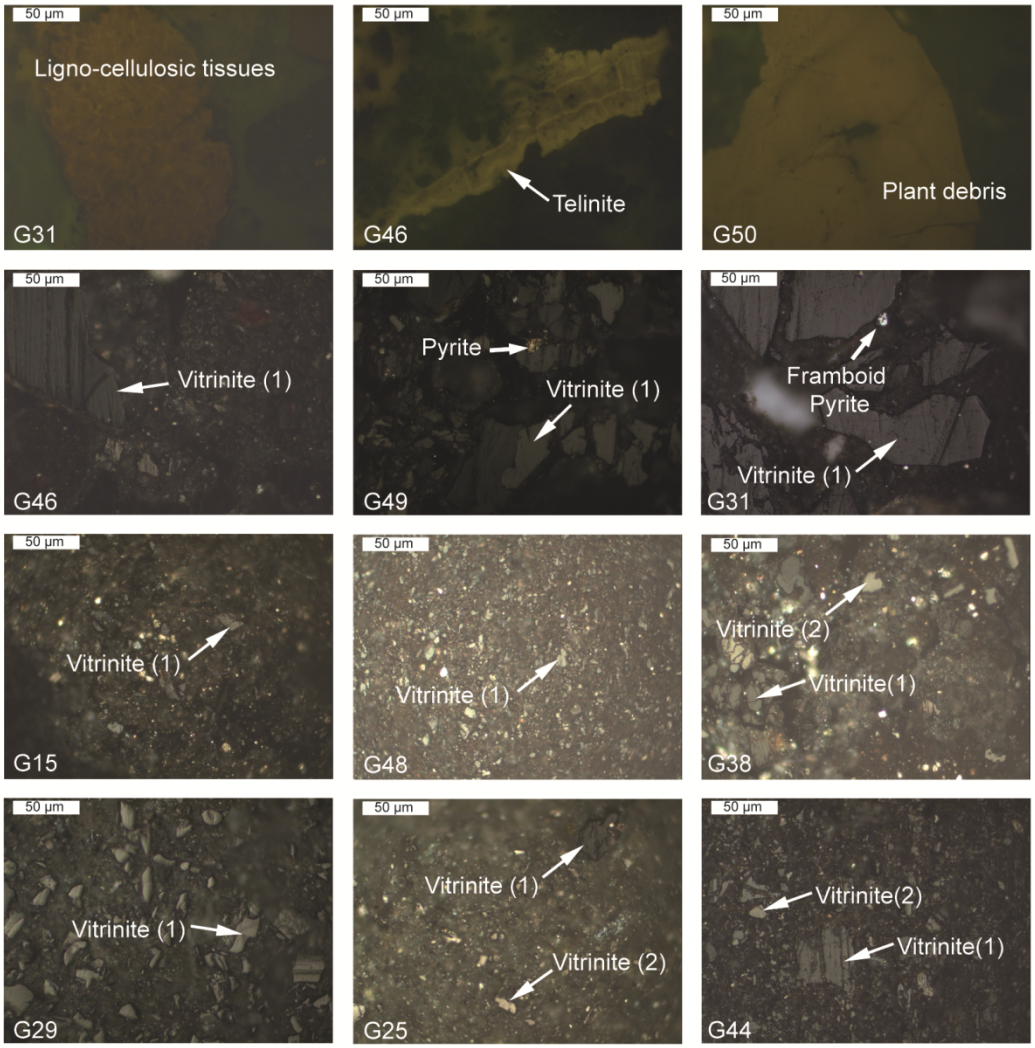

bre_12439_f3.tif

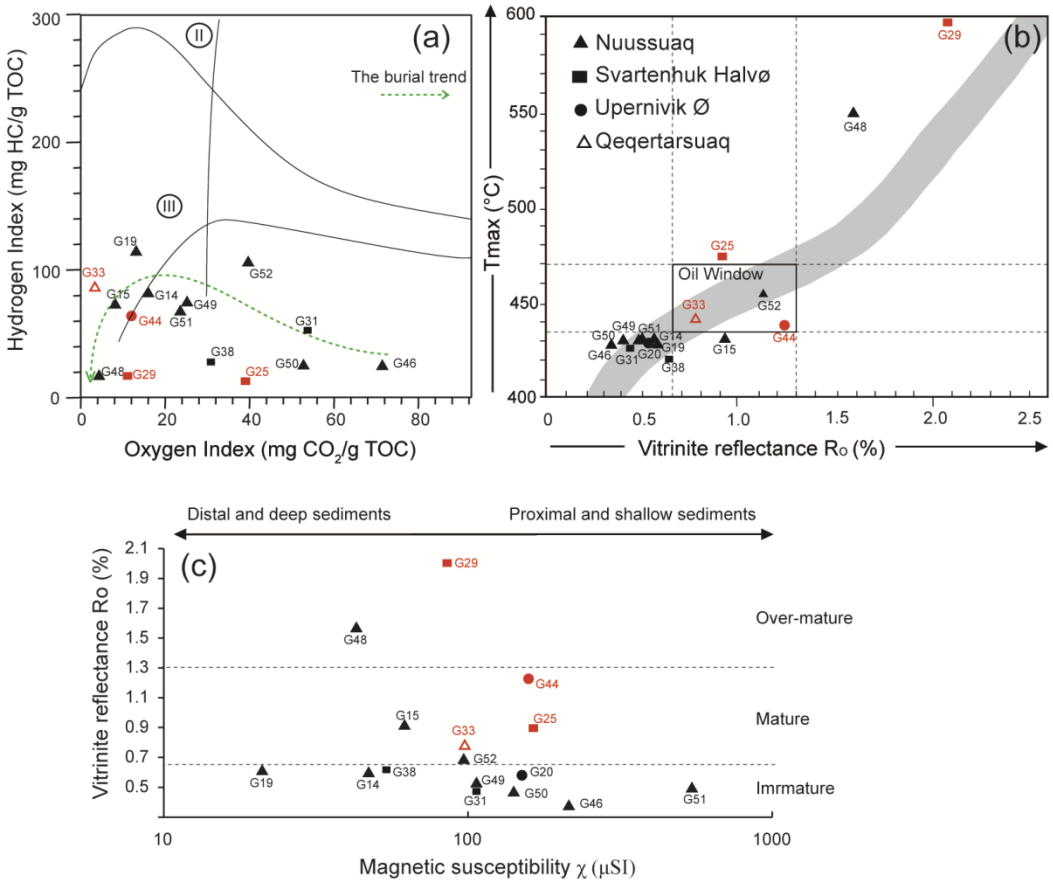

bre_12439_f4.tif

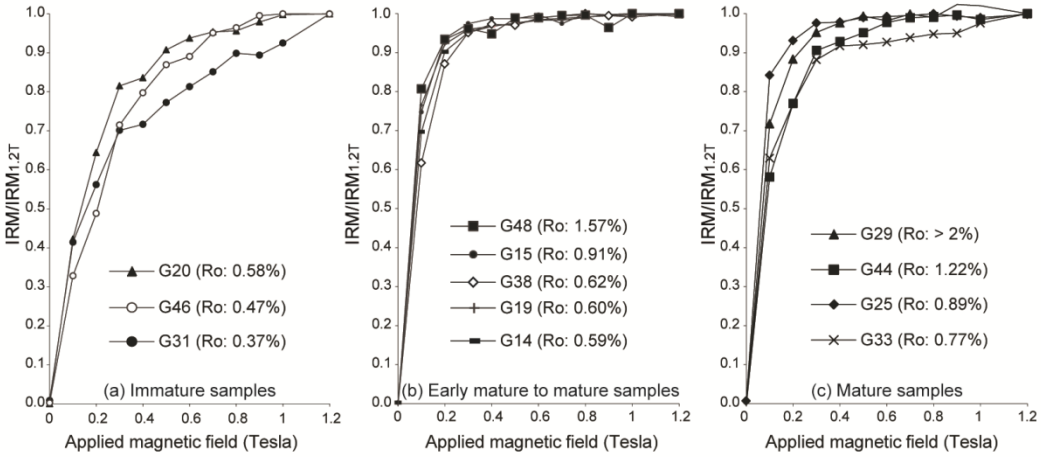

bre_12439_f5.tif

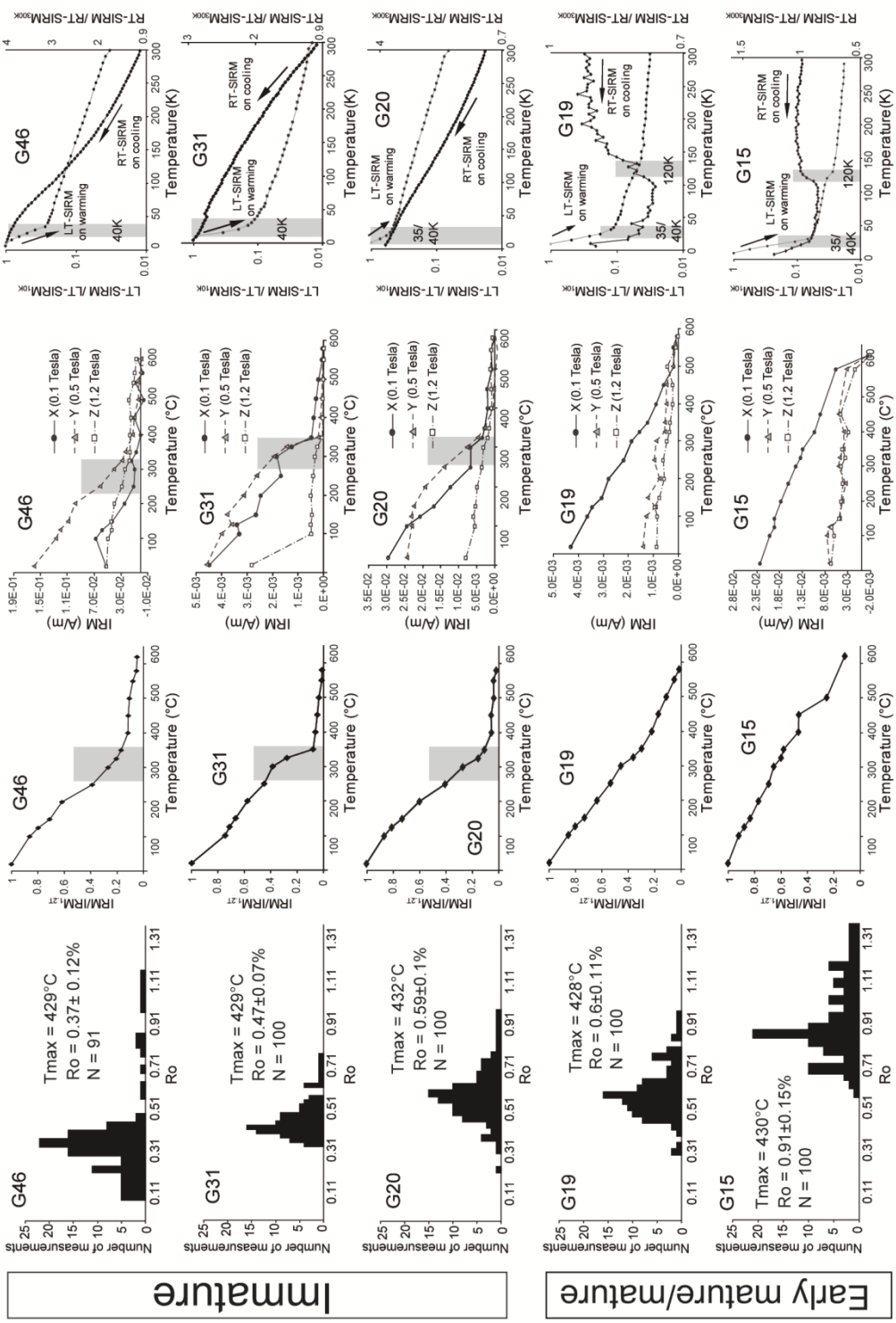

bre_12439_f6.tif

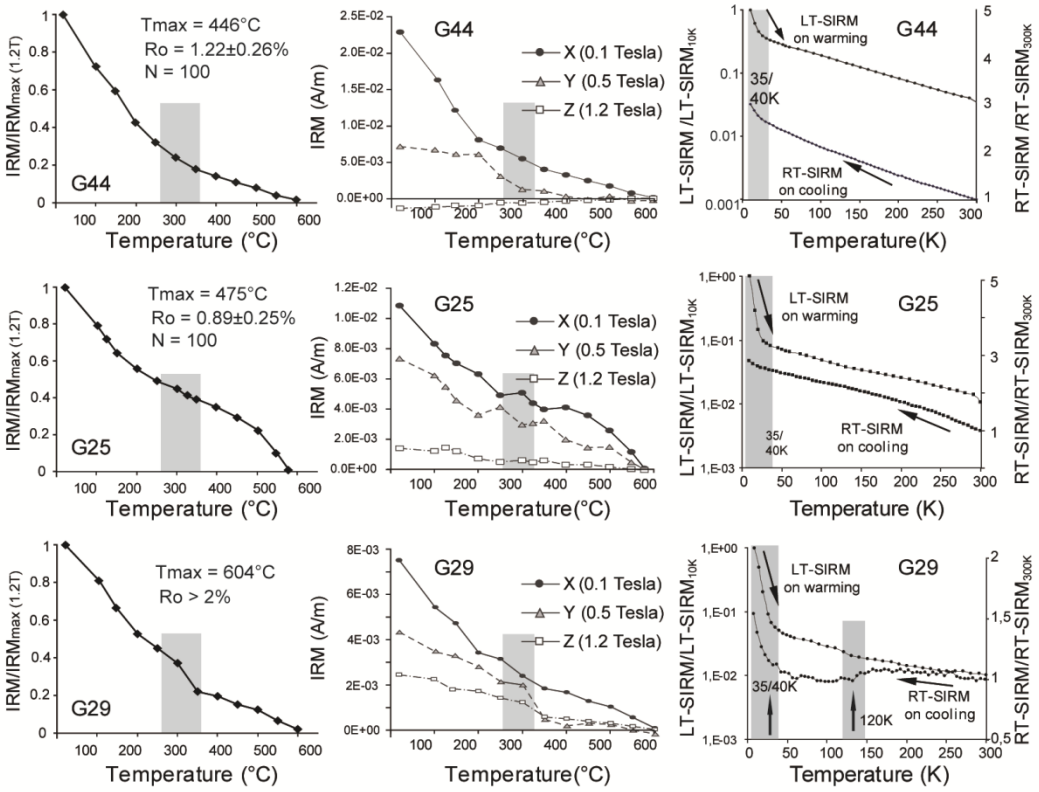

(a) High temperature normalized magnetic curves

(b) High temperature magnetic curves

(c) Low temperature magnetic curves

bre_12439_f7.tif

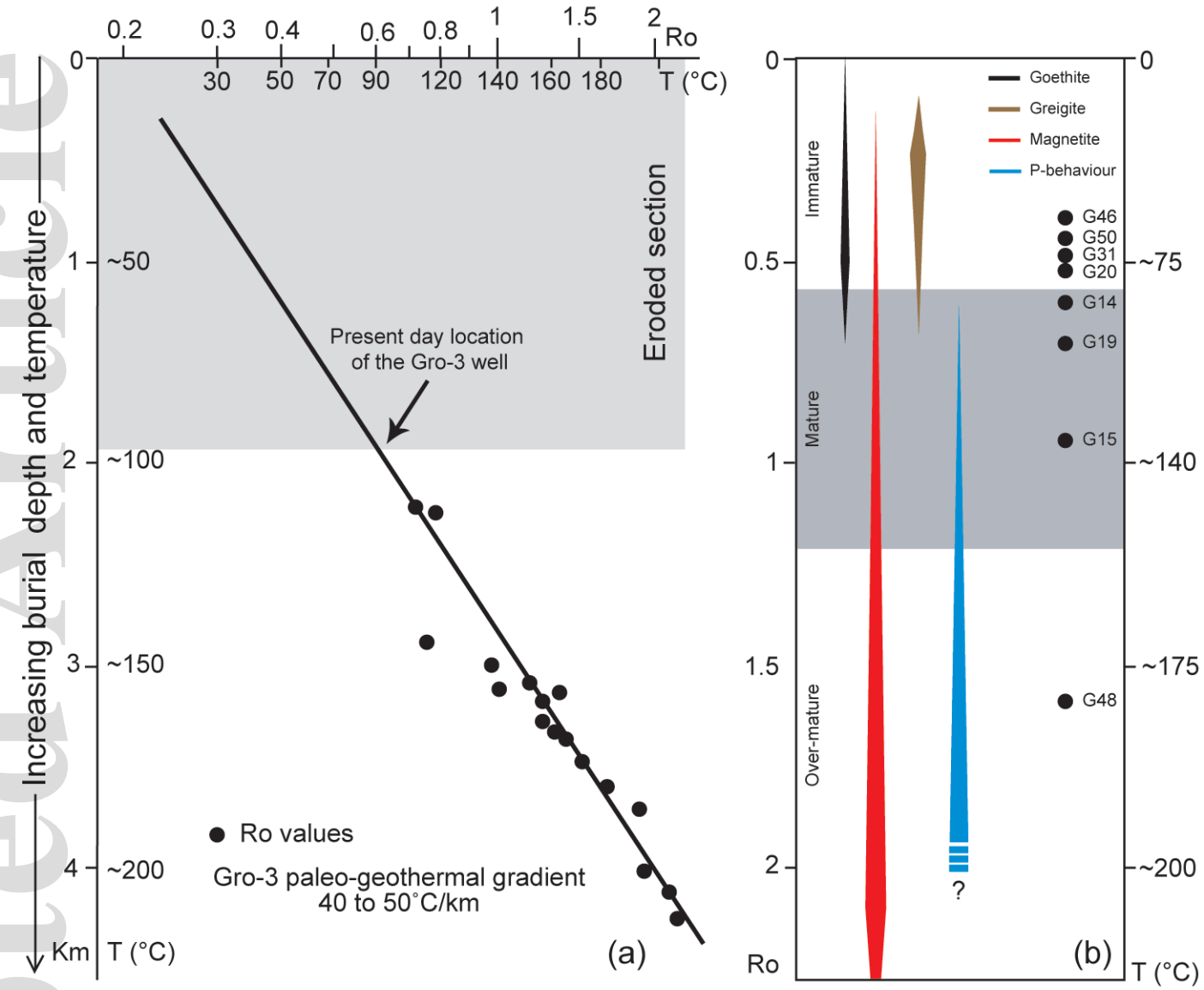

bre_12439_f8.tif

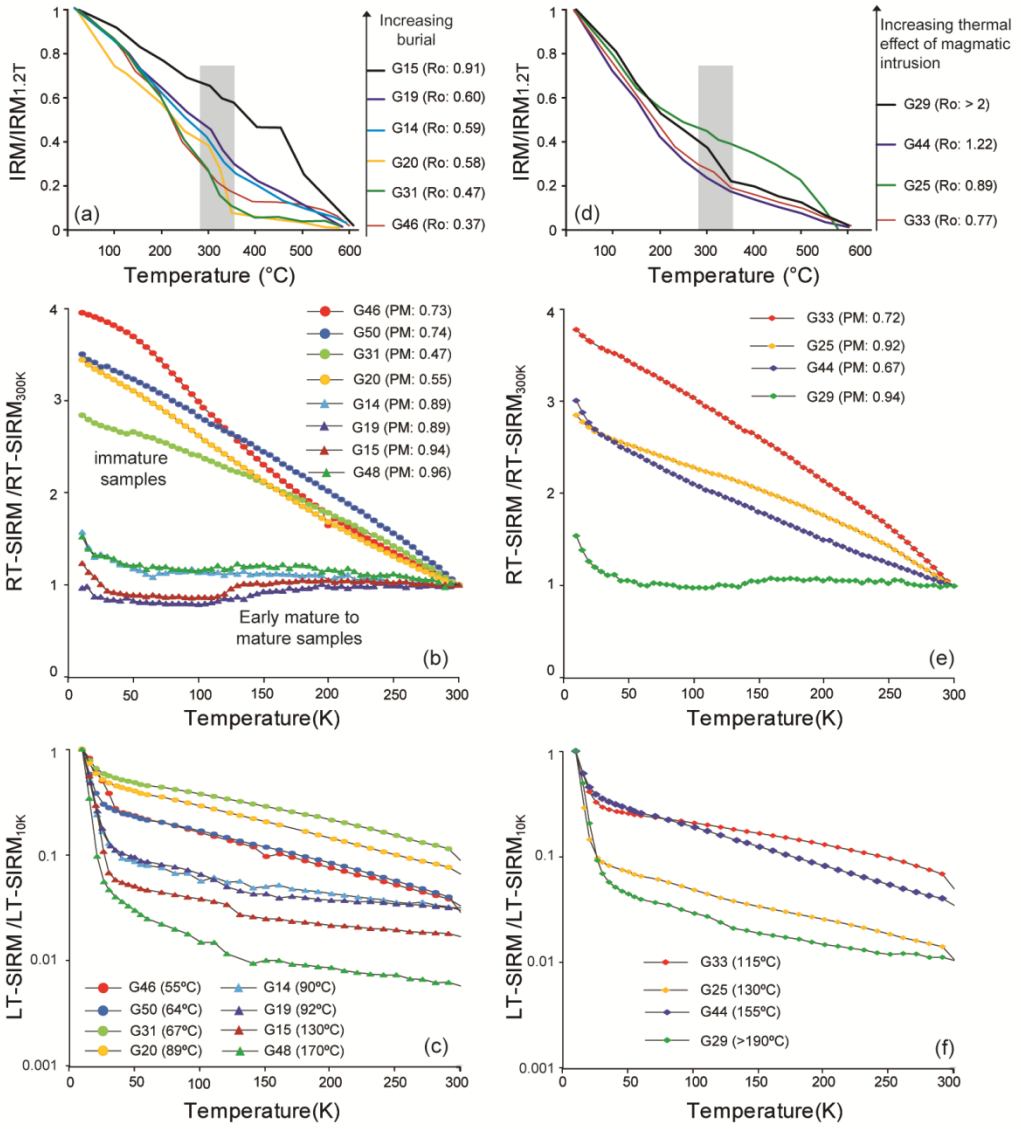

bre_12439_f9.tif